ORGANOMETALLICS

Article

pubs.acs.org/Organometallics

Coordinating Tectons: Bimetallic Complexes from Bipyridyl Terminated Group 8 Alkynyl Complexes

George A. Koutsantonis,*[,†] Paul J. Low,*[,†,‡] Campbell F. R. Mackenzie,[†] Brian W. Skelton,[†,§] and Dmitry S. Yufit[‡]

[†]Chemistry, School of Chemistry and Biochemistry and [§]Centre for Microscopy, Characterisation and Analysis, University of Western Australia, Crawley, Western Australia 6009, Australia

[‡]Department of Chemistry, Durham University, South Road, Durham DH1 3LE, U.K.

Supporting Information

ABSTRACT: Bipyridyl appended ruthenium alkynyl complexes have been used to prepare a range of binuclear homometallic ruthenium and heterometallic ruthenium−rhenium complexes. The two metal centers are only weakly coupled, as evinced by IR and UV−vis−near NIR spectroelectrochemical experiments and supported by quantum chemical calculations. The alkynyl complexes of the type [Ru(C≡Cbpy){L_n}] ({L_n} = {$(PPh_3)_2Cp$}, {(dppe)Cp*}, {$Cl(dppm)_2$}) undergo reversible one-electron oxidations centered largely on the alkynyl ligands, as has been observed previously for closely related complexes. The homometallic binuclear complexes, exemplified by [Ru(C_2bpy-κ^2-$N'N$-RuClCp)$(PPh_3)_2$Cp] undergo two essentially reversible oxidations, the first centered on the (C_2bpy-κ^2-$N'N$-RuClCp) moiety and the second on the Ru(C≡Cbpy)$(PPh_3)_2$Cp fragment, leading to radical cations that can be described as Class II mixed-valence complexes. The heterometallic binuclear complexes [Ru(C_2bpy-κ^2-$N'N$-ReCl$(CO)_3$){L_n}] display similar behavior, with initial oxidation on the ruthenium fragment giving rise to a new optical absorption band with Re → Ru(C≡Cbpy) charge transfer character. The heterometallic complexes also exhibit irreversible reductions associated with the Re hetereocycle moiety.

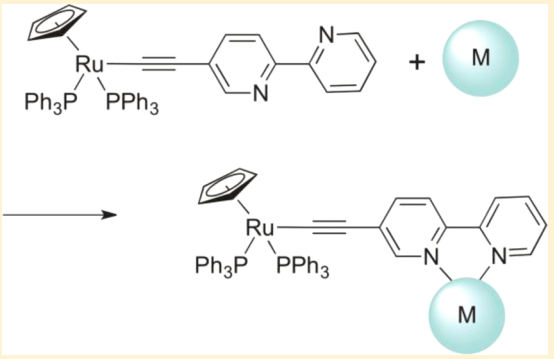

INTRODUCTION

Molecular electronics involves the use of individual molecules, or groups of molecules, as functional moieties that may replace or augment conventional solid-state (usually silicon) electronic components, and is widely regarded as the ultimate solution to the growing difficulties facing "top-down" design strategies.[1−7] In the construction of hybrid molecular/solid-state electronic devices, the key challenge lies in the realization of the potential of single-electron phenomena within hybrid device structures.[8,9] There needs elementary science to be developed that investigates the fundamental properties of molecules, including electronic coupling effects, to realize molecule-based electronics technology.

Many prototypical bimetallic systems have been investigated to define intramolecular, solution-phase electron transfer characteristics and identify promising candidate wire-like molecular moieties,[10−12] such as polyynes[13−16] and oligo-(phenylene)ethynylene based structures[17] and which have successfully been translated into designs of organic and organometallic molecules for study as components in molecular junctions.[18−23]

In this regard, the use of organometallic coordinating tectons in the assembly of large heterometallic complexes, albeit not with wire-like geometries, by Lang provides conceptual basis for further development of these synthetic strategies.[24,25] Our proposed organometallic-coordination polymer approach to molecular electronic components involves the preparation of modular organometallic "coordinating tectons" that will be used as the basic repeating unit to form polymetallic complexes of well-defined length.

Initially, our interest lies in complexes where spectroscopic, including spectroelectrochemical, and computational methods will be used to explore molecular electronic structure as a function of conformation and redox state in these systems and assess the influence of conformation on intramolecular charge transfer process.

Herein we describe further steps toward this goal and detail the preparation of a series of complexes whose role as putative tectons and molecular electronic structure is investigated through the formation of bimetallic complexes.

EXPERIMENTAL SECTION

General Considerations. All reactions were performed under an atmosphere of high purity argon or nitrogen using standard Schlenk techniques. Reaction solvents either were purified and dried using an

Special Issue: Organometallic Electrochemistry

Received: February 16, 2014
Published: August 6, 2014

   dx.doi.org/10.1021/om500172r | *Organometallics* 2014, 33, 4911−4922

Innovative Technology SPS-400 (THF, ether, hexane, and toluene) and degassed prior to use or were purified and dried by appropriate[26] means prior to distillation and storage under Argon. No special precautions were taken to exclude air or moisture during workup. The compounds [*trans*-Ru(C≡Cbpy)Cl(dppm)$_2$] (**3**),[27] [RuCl(COD)Cp],[28] [RuCl(PPh$_3$)$_2$Cp],[29] [RuCl(dppe)Cp*],[30] [Re(κ^2-*N*′*N*-HC$_2$bpy)Cl(CO)$_3$],[31] HC≡Cbpy,[32,33] and PhC≡Cbpy[34] were synthesized according to literature procedures (HC≡Cbpy = 5-ethynyl-2,2′-bipyridine; PhC≡Cbpy = 5-(phenylethynyl)-2,2′-bipyridine). All other materials were obtained from commercial suppliers and used as received.

The NMR spectra were recorded on 400 MHz Varian, Bruker AV-500, or Bruker AV-600 spectrometers. ^{1}H and ^{13}C{^{1}H} spectra were referenced to residual solvent signals, whereas ^{31}P{^{1}H} spectra were referenced to external phosphoric acid. IR spectra were recorded using a Thermo Scientific Nicolet 6700 spectrometer as CH_2Cl_2 solutions in a cell fitted with CaF_2 windows. UV−vis spectra were recorded on a PerkinElmer Lambda 25 UV−vis spectrophotometer as CH_2Cl_2 solutions in a quartz cell, or on a Thermo Array UV−vis spectrophotometer as CH_2Cl_2 solutions in a cell with CaF_2 windows. MALDI-mass spectra were recorded using an Autoflex II TOF/TOF mass spectrometer with a 337 nm laser. Samples in CH_2Cl_2 (1 mg/mL) were mixed with a matrix solution of trans-2-[3-(4-*tert*-butylphenyl)-2-methyl-2-propenylidene]malononitrile (DCTB) in a 1:9 ratio, with 1 μL of mixture spotted onto a metal target prior to exposure to the MALDI ionization source. Electrospray mass spectra were recorded on a Waters LCT Premier spectrometer. Microanalytical Services, Research School of Chemistry, Australian National University, Canberra, Australia, or London Metropolitan University, London, United Kingdom, performed elemental analyses.

Electrochemical analyses were carried out using either an EcoChemie Autolab PG-STAT 30 or a Palm Instruments EmStat potentiostat. A platinum disk electrode with platinum counter and platinum pseudoreference electrodes were used in CH_2Cl_2 solutions containing 0.1 M ^{n}Bu$_4$NPF$_6$ electrolyte. The decamethylferrocene/decamethylferrocenium ($FeCp^*_2$/[$FeCp^*_2$]$^+$) couple was used as an internal reference, with all potentials reported relative to the ferrocene/ferrocenium couple ($FeCp_2$/[$FeCp_2$]$^+$) ($FeCp^*_2$/[$FeCp^*_2$]$^+$ = −0.48 V in CH_2Cl_2). Spectroelectrochemical measurements were made in an OTTLE cell of Hartl design,[35] from CH_2Cl_2 solutions containing 0.1 M ^{n}Bu$_4$NPF$_6$ electrolyte. The cell was fitted into the sample compartment of the Thermo 6700 FTIR or Cary 5000 UV−vis−near NIR spectrophotometer, and electrolysis in the cell was performed with either a PGSTAT-30 or EmStat potentiostat.

Crystallography. The crystal data for **1**−**3**, **5**−**7**, **9**, **10**, **12**−**15** are summarized in Table S2 (Supporting Information) with the complexes depicted in Chart 1 and in the figures below, where ellipsoids have been drawn at the 50% probability level, unless otherwise stated. Crystallographic data for the structures were collected at 100(2) K (180 K for **3b**) on an Oxford Diffraction Gemini diffractometer fitted with Cu Kα radiation (for **2**, **3.2Tol**, **3b**, **12**) or Mo Kα (**1**,**10**, and **13**). Data for **9**, **14**, and **15** were collected on an Oxford Diffraction XCalibur diffractometer fitted with Mo Kα radiation Following analytical absorption corrections and solution by direct methods, the structures were refined against F^2 with full-matrix least-squares using the program SHELXL-97.[36] Ligand nitrogen atoms were distinguished from carbon atoms on the basis of geometries and refinement. All hydrogen atoms were added at calculated positions and refined by use of riding models with isotropic displacement parameters based on those of the parent atoms. Except were mentioned below, anisotropic displacement parameters were employed throughout for the non-hydrogen atoms. All H atoms were added at calculated positions and refined by use of a riding model with isotropic displacement parameters based on the isotropic displacement parameter of the parent atom. For complex **3**, two structures were obtained and, in the one containing disordered toluene solvent, one of the two solvent toluene molecules was modeled as being disordered over two sets of sites each with site occupancies set at 0.5 after trial refinement. In the other, **3b**, one of the bipyridyl rings was similarly modeled as disordered. Geometries of the disordered atoms were restrained to ideal values. Non-H atoms of the disordered atoms were refined with isotropic displacement parameters only.

Chart 1. Complexes Prepared and Studied in This Work

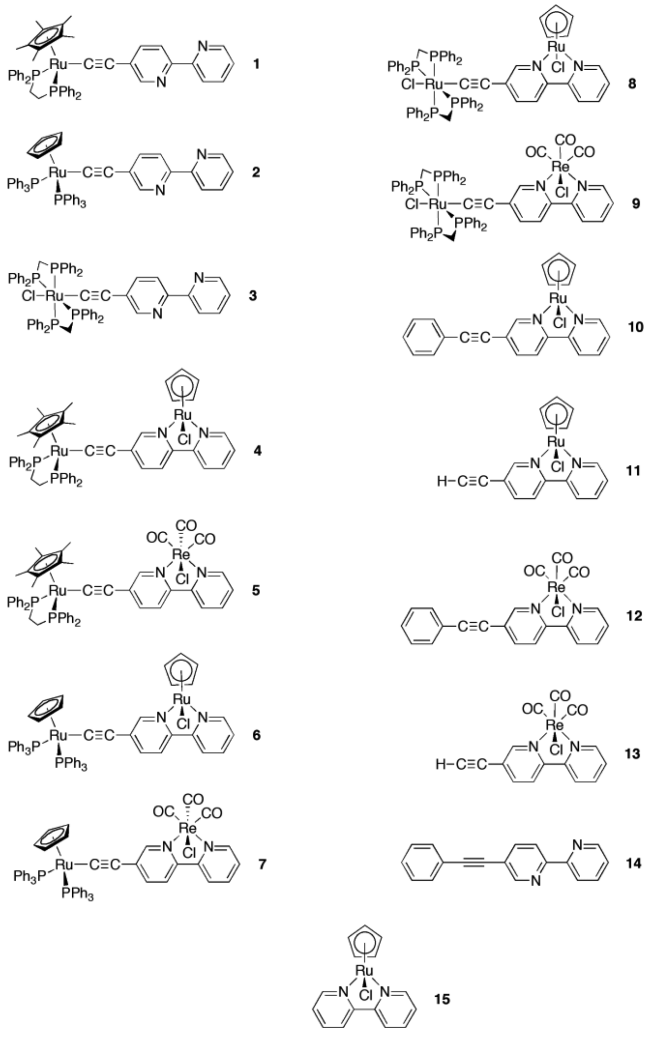

In the structure of **9**, three of the dichloromethane solvent molecules were modeled as being disordered. Their geometries were restrained to ideal values.

The data for compounds **5** and **7** were collected at 120 and 100 K, respectively, on a Rigaku Saturn 724+ diffractometer at Station I19 of the Diamond Light Source synchrotron (undulator, l = 0.6889 Å, w-scan, 1.0°/frame). The data for compound **6** were collected on a Bruker SMART CCD 6000 diffractometer (graphite monochromator, $\lambda_{\text{Mo K}\alpha}$, λ = 0.71073 Å) at 100 K. The structures were solved by direct methods and refined by full-matrix least-squares on F^2 for all data using SHELXTL[36] and OLEX2.[37]

Synthesis of the Complexes. *[Ru(C≡Cbpy)(dppe)Cp*] (1).* [RuCl(dppe)Cp*] (200 mg, 0.298 mmol), HC≡Cbpy (65 mg, 0.359 mmol), and NH_4PF_6 (100 mg, 0.613 mmol) were suspended in dry MeOH (40 mL) and heated to reflux for 2 h, during which a yellow suspension became a deep red solution. The solution was cooled to room temperature before the addition of DBU, followed by 30 min of stirring, resulting in the formation of an orange precipitate. The mixture was cooled to 0 °C, and the reaction product was collected on a glass frit and washed with MeOH (2 × 3 mL) and Et_2O (3 mL) to give the product as an orange powder (214 mg, 88%). Crystals suitable for X-ray analysis were grown through the vapor diffusion of *n*-pentane into a CH_2Cl_2 solution of the complex. Anal. Calcd for $C_{48}H_{46}N_2P_2Ru_1$: C, 70.83; H, 5.70; N, 3.44. Found: C, 70.77; H, 5.64; N, 3.52. ^{1}H NMR ($CDCl_3$, 400 MHz): 1.57 (s, 15H, Cp*), 2.01−2.15 (m, 2H, PCH_2CH_2P), 2.63−2.73 (m, 2H, PCH_2CH_2P),

dx.doi.org/10.1021/om500172r | *Organometallics* 2014, 33, 4911−4922

7.05 (d, 1H, H5′), 7.19 (m, 1H, H4′), 7.22−7.26 (m, 8H, H_{meta}), 7.29−7.40 (m, 9H, H_{ortho} and H3′), 7.73−7.76 (m, 4H, H_{para}), 8.02 (s, 1H, H6), 8.08 (d, 1H, H4, $^3J_{HH}$ = 8 Hz), 8.25 (d, 1H, H3, $^3J_{HH}$ = 8 Hz), 8.61 (dd, 1H, H6′). $^{13}C\{^1H\}$ NMR ($CDCl_3$, 100 MHz): 10.0 (s, Me_5Cp), 29.4 (m, PCH_2CH_2P), 92.8 (s, Me_5Cp), 107.7 (s, C_β), 120.1(s, C3), 120.6 (s, C3′), 122.5 (s, C5′), 127.4 (t, Ph_{meta}), 127.6 (t, Ph_{meta}), 129.2 (s, Ph_{para}), 133.3 (t, Ph_{ortho}), 136.4 (s, C5), 136.8 (s, C4′) 137.4 (s, C4), 138.7 (dd, C_{ipso}, $^1J_{CP}$ = 39.7 Hz, $^4J_{CP}$ = 6.4 Hz), 141.0 (t, C_α, $^2J_{CP}$ = 24.4 Hz), 149.0 (s, C2), 149.1 (s, C6′), 151.0 (s, C6), 157.0 (s, C2′). $^{31}P\{^1H\}$ NMR ($CDCl_3$, 162 MHz): 79.72 ppm (s). IR (CH_2Cl_2 solution): $\nu_{C\equiv C}$ 2067 cm^{-1} (2044 cm^{-1} shoulder). MS (MALDI): m/z 814 ($[M]^+$, 100%), 663 ($[Ru(CO)(dppe)Cp^*]^+$, 90%), 635 ($[Ru(dppe)Cp^*]^+$, 30%). UV−vis (CH_2Cl_2) λ (nm) [$\varepsilon \times 10^4$ M^{-1} cm^{-1}]: 399 [2.37].

*[Ru(C≡Cbpy)(PPh$_3$)$_2$Cp] (**2**).* [$RuCl(PPh_3)_2Cp$] (400 mg, 0.551 mmol), HC≡Cbpy (150 mg, 0.826 mmol), and NH_4PF_6 (200 mg, 1.23 mmol) were refluxed in MeOH for 2 h, during which the yellow suspension became a deep red solution. The solution was cooled to room temperature before the addition of DBU (0.5 mL), followed by 30 min of stirring, resulting in the formation of a yellow precipitate. The mixture was cooled to 0 °C, and the reaction product was collected on a glass frit and washed with MeOH (2 × 5 mL) to give the product as a yellow powder (348 mg, 73%). Crystals suitable for X-ray analysis were obtained through the slow diffusion of hexane into a $CDCl_3$ solution of the complex. This complex matches the spectroscopic data presented previously,[31] with the following revised $^{13}C\{^1H\}$ assignments; $^{13}C\{^1H\}$ ($CDCl_3$, 151 MHz): δ 85.5 (s, Cp), 112.2 (s, C_β), 120.3 (s, C3), 120.8 (s, C3′), 122.7 (s, C5′), 127.2 (s, C5), 127.3 (t, $^2J_{CP}$ = 4.4 Hz, C_{ortho}), 128.4 (t, $^2J_{CP}$ = 25.7 Hz, C_α), 128.7 (s, C_{para}), 133.9 (t, $^3J_{CP}$ = 4.8 Hz, C_{meta}), 136.8 (s, C4′), 138.0 (s, C4), 138.8 (t, $^1J_{CP}$ = 21.0 Hz, C_{ipso}), 149.2 (s, C6′), 149.7 (s, C2), 151.2 (s, C6), 156.9 (s, C2′).

[Ru(C≡Cbpy-κ^2-N′N-RuClCp)(dppe)Cp] (**4**).* [Ru(C≡Cbpy)-(dppe)Cp*](**1**) (50 mg, 0.061 mmol) and [RuCl(COD)Cp] (20 mg, 0.065 mmol) were dissolved in acetone (30 mL) and stirred at room temperature overnight. The solvent volume was reduced to ca. 10 mL in vacuo, followed by the addition of diethyl ether (30 mL) and cooling to −15 °C. The precipitate that formed was collected and washed with diethyl ether (2 × 5 mL) to give the product as purple crystals (43 mg, 69%). Anal. Calcd for $C_{53}H_{51}ClN_2P_2Ru_2$: C, 62.68; H, 5.06; N, 2.76. Found: C, 62.55; H, 4.95; N, 2.86. ^1H NMR (CD_2Cl_2, 600 MHz): 1.59 (s, 15H, Cp*), 2.16 (m, 2H, PCH_2CH_2P), 2.68 (m, 2H, PCH_2CH_2P), 4.11 (s, 5H, Cp), 6.92 (d, 1H, H3′), 7.18 (ddd, 1H, H5′), 7.21−7.29 (m, 4H, H_{meta}), 7.33−7.43 (m, 8H, H_{ortho} and H_{meta}), 7.44−7.48 (m, 4H, H_{para}), 7.60 (d, 1H, H4, $^3J_{HH}$ = 8.4 Hz), 7.65 (ddd, 1H, H4′), 7.72−7.80 (m, 5H, H_{ortho} and H3), 8.79 (s, 1H, H6), 9.50 (d, 1H, H6′). $^{13}C\{^1H\}$ NMR (CD_2Cl_2, 151 MHz): δ 10.2 (s, Me_5Cp), 29.8 (m, PCH_2CH_2P), 69.2 (s, Cp), 93.5 (s, Me_5Cp), 108.6 (s, C_β), 120.8 (s, C3), 121.1 (s, C3′), 123.4 (s, C5′), 127.9 (m, C_{meta}), 129.1 (s, C5), 129.6 (m, C_{para}), 133.7 (m, C_{ortho}), 134.6 (s, C4′), 135.8 (s, C4), 138.8 (dd, C_{ipso}, $^1J_{CP}$ = 72.9 Hz, $^4J_{CP}$ = 34.0 Hz), 148.7 (s, C2), 150.1 (t, C_α, $^2J_{CP}$ = 24.0 Hz), 155.1 (s, C6′), 156.0 (s, C6), 156.8 (s, C2′). $^{31}P\{^1H\}$ NMR (CD_2Cl_2, 243 MHz): 81.17 (d, $^3J_{PP}$ = 16 Hz), 80.90 (d, $^3J_{PP}$ = 16 Hz). IR (CH_2Cl_2 solution): $\nu_{C\equiv C}$ 2042 cm^{-1}. MS (MALDI): m/z 981 ($[M - Cl]^+$, 100%), 663 ($[Ru(CO)(dppe)Cp^*]^+$, 50%), 635 ($[Ru(dppe)Cp^*]^+$, 30%), 1015 ($[M]^+$, 10%), 814 ($[M - RuClCp]^+$, 10%). UV−vis (CH_2Cl_2) λ (nm) [$\varepsilon \times 10^4$ M^{-1} cm^{-1}]: 299 [1.75], 367 [1.42], 450 [1.84].

[Ru(C≡Cbpy-κ^2-N′N-ReCl(CO)$_3$)(dppe)Cp] (**5**).* [Ru(C≡Cbpy)-(dppe)Cp*](**1**) (70 mg, 0.086 mmol) and [$ReCl(CO)_5$] (33 mg, 0.091 mmol) were dissolved in toluene (40 mL), and the solution was refluxed for 2 h, during which a bright yellow solution became deep purple. The solvent volume was reduced to ca. 10 mL in vacuo, followed by the addition of hexane (20 mL) and cooling to 0 °C. The precipitate was collected and washed with hexane (3 × 3 mL) to give the product as purple crystals (77 mg, 80%). Crystals suitable for X-ray analysis were obtained through the slow diffusion of hexane into a $CDCl_3$ solution of the complex. Anal. Calcd for $C_{51}H_{46}ClN_2O_3P_2Re_1Ru_1$: C, 54.71; H, 4.14; N, 2.50. Found: C, 54.78; H, 4.12; N, 2.60. ^1H NMR (CD_2Cl_2, 600 MHz): δ 1.60 (s, 15H Cp*), 2.11−2.21 (m, 2H, PCH_2CH_2P), 2.61−2.69 (m, 2H, PCH_2CH_2P), 7.06 (dd, 1H, H3′), 7.15 (ddd, 1H, H5′), 7.18 (d, 1H, H4), 7.22−7.41 (m, 12H, H_{ortho} and H_{para}), 7.41−7.46 (m, 4H, H_{meta}), 7.67−7.73 (m, 4H, H_{meta}), 7.89−7.94 (m, 2H, H4′ and H3), 8.18 (s, 1H H6), 8.88 (dd, 1H, H6′). $^{13}C\{^1H\}$ NMR (CD_2Cl_2, 151 MHz): δ 10.0 (s, Me_5Cp), 29.7 (m, PCH_2CH_2P), 93.9 (s, Me_5Cp), 110.2 (s, C_β), 122.1 (s, C3), 122.7 (s, C3), 125.2 (s, C5′), 128.1 (m, C_{ortho}), 129.7 (m, C_{para}), 131.4 (s, C5), 133.5 (s, C_{meta}), 136.3 (m, C_{ipso}), 138.5 (s, C4′), 139.0 (s, C4), 147.0 (s, C2), 152.9 (s, C6′), 154.3 (s, C2′), 156.9 (s, C2′), 160.0 (m, C_α), 190.7 (s, CO), 198.4 (s, CO). $^{31}P\{^1H\}$ NMR (CD_2Cl_2, 243 MHz): 80.86 (d, $^3J_{PP}$ = 16 Hz), 80.62 (d, $^3J_{PP}$ = 16 Hz). IR (CH_2Cl_2 solution): $\nu_{C\equiv C}$ 2038 cm^{-1}, $\nu_{C\equiv O}$ 2018 cm^{-1}, $\nu_{C\equiv O}$ 1915 cm^{-1}, and $\nu_{C\equiv O}$ 1893 cm^{-1}. MS (MALDI): m/z 663 ($[Ru(CO)(dppe)Cp^*]^+$, 100%), 635 ($[Ru(dppe)Cp^*]^+$, 70%), 1120 ($[M]^+$, 5%). UV−vis (CH_2Cl_2) λ (nm) [$\varepsilon \times 10^4$ M^{-1} cm^{-1}]: 387 [1.21], 506 [1.72].

*[Ru(C≡Cbpy-κ^2-N′N-RuClCp)(PPh$_3$)$_2$Cp] (**6**).* [Ru(C≡Cbpy)-(PPh_3)$_2$Cp] (**2**) (100 mg, 0.115 mmol) and [RuCl(COD)Cp] (38 mg, 0.123 mmol) were dissolved in acetone (30 mL), and the solution was stirred at room temperature overnight. The solvent volume was reduced to ca. 10 mL in vacuo, followed by the addition of diethyl ether (30 mL) and cooling to −15 °C. The precipitate that formed was collected and washed with diethyl ether (2 × 5 mL) to give the product as purple crystals (92 mg, 75%). Crystals suitable for X-ray analysis were obtained through layer diffusion of hexane into a CH_2Cl_2 solution of the complex. Anal. Calcd for $C_{58}H_{47}ClN_2P_2Ru_2$: C, 65.01; H, 4.42; N, 2.61. Found: C, 64.89; H, 4.51; N, 2.53. ^1H NMR (CD_2Cl_2, 500 MHz): δ 4.18 (s, 5H, Cp_{bpy}), 4.42 (s, 5H, Cp_{PP}), 7.13−7.21 (m, 13H, H_{meta} and H5′), 7.26−7.30 (m, 7H, H_{para} and H3′), 7.43−7.52 (m, 12H, H_{ortho}), 7.68 (dd, (1H, H4′), 7.75 (d, 1H, H3), 7.84, (d, 1H, H4), 9.29, (d, 1H, H6), 9.55 (d, 1H, H6′). $^{13}C\{^1H\}$ NMR (CD_2Cl_2, 126 MHz): δ 69.3 (s, Cp_{bpy}), 86.1 (s, Cp_{PP}), 112.6 (s, C_β), 121.0 (s, C3), 121.3 (s, C3′), 123.6 (s, C5′), 127.8 (m, C_{meta}), 128.5 (s, C5), 129.2 (s, C_{para}), 134.6 (m, C_{ortho} and C4′), 135.7 (s, C4), 137.0 (t, C_α, $^2J_{CP}$ = 24.3 Hz), 138.9 (m, C_{ipso}), 149.3 (s, C2), 155.2 (s, C6′), 156.7 (m, C6 and C2′). $^{31}P\{^1H\}$ NMR ($CDCl_3$, 162 MHz): δ 49.29 (s), 49.26 (s). IR (CH_2Cl_2 solution): $\nu_{C\equiv C}$ 2045 cm^{-1}. MS (MALDI): m/z 719 ($[Ru(CO)(PPh_3)_2Cp]^+$, 100%), 1036 ($[M - Cl]^+$, 15%), 774 ($[M - PPh_3 - Cl]^+$, 12%), 1072 ($[M + H]^+$, 5%). UV−vis (CH_2Cl_2) λ (nm) [$\varepsilon \times 10^4$ M^{-1} cm^{-1}]: 295 [2.43], 374 [1.31], 434 [2.36].

*[Ru(C≡Cbpy-κ^2-N′N-ReCl(CO)$_3$)(PPh$_3$)$_2$Cp] (**7**).* [Ru(C≡Cbpy)-(PPh_3)$_2$Cp] (**2**) (55 mg, 0.063 mmol) and [$ReCl(CO)_5$] (26 mg, 0.072 mmol) were dissolved in toluene (30 mL), and the solution was refluxed for 2 h, during which a bright yellow solution became deep red. The solvent volume was reduced to ca. 5 mL in vacuo, followed by the addition of hexane (20 mL) and cooling to −15 °C overnight. The precipitate that formed was collected and washed with hexane (3 × 5 mL) to give the product as a red powder (38 mg, 51%). Crystals suitable for X-ray crystallography were grown through vapor diffusion of *n*-pentane into a CD_2Cl_2 solution of the compound. Anal. Calcd for $C_{56}H_{42}ClN_2O_3P_2ReRu{\cdot}1.5CH_2Cl_2$: C, 53.00; H, 3.48; N, 2.15. Found: C, 53.40; H, 3.25; N, 2.14. ^1H NMR: δ 4.43 (s, 5H, Cp), 7.10 (ddd, 1H, H5′), 7.15−7.18 (m, 12H, H_{ortho}), 7.26−7.29 (m, 6H, H_{para}), 7.38−7.45 (m, 13H, H_{meta} and H3′), 7.89 (d, 1H, H4), 8.00 (m, 2H, H3 and H4′), 8.63 (d, 1H, H6), 8.94 (d, 1H, H6′). $^{13}C\{^1H\}$ NMR (CD_2Cl_2, 151 MHz): δ 86.4 (s, Cp), 113.7 (s, C_β), 122.3 and 122.9 (s, C3 and C3′), 125.5 (s, C5′), 127.9 (s, C_{ortho}), 129.3 (s, C_{para}), 130.8 (s, C4′), 131.6 (s, C4), 132.3 (s, C5), 134.0 (m, C_{meta}), 138.8 (m, C_{ipso}), 146.6 (m, C_α), 147.8 (s, C2), 153.0 (s, C6′), 154.6 (s, C6), 156.8 (s, C2′), 190.6 (s, CO), 198.4 (s, CO). $^{31}P\{^1H\}$ NMR ($CDCl_3$, 162 MHz): δ 49.1 (s). IR (CH_2Cl_2 solution): $\nu_{C\equiv C}$ 2043 cm^{-1}, $\nu_{C\equiv O}$ 2019 cm^{-1}, $\nu_{C\equiv O}$ 1916 cm^{-1} and $\nu_{C\equiv O}$ 1894 cm^{-1}. MS (MALDI): m/z 719 ($[Ru(CO)(PPh_3)_2Cp]^+$, 100%), 691 ($[Ru(PPh_3)_2Cp]^+$, 20%), 1140 ($[M - Cl]^+$, 5%). UV−vis (CH_2Cl_2) λ (nm) [$\varepsilon \times 10^4$ M^{-1} cm^{-1}]: 302 [1.98], 481 [1.79].

*[Ru(C≡Cbpy-κ^2-N′N-RuClCp)Cl(dppm)$_2$](**8**).* [Ru(C≡Cbpy)Cl-($dppm)_2$] (85 mg, 0.078 mmol) and [RuCl(COD)Cp] (30 mg, 0.097 mmol) were dissolved in acetone (15 mL), and the solution was stirred at room temperature overnight. The solvent volume was

dx.doi.org/10.1021/om500172r | *Organometallics* 2014, 33, 4911−4922

reduced to ca. 5 mL in vacuo, and the precipitate was collected and washed with diethyl ether (3 × 3 mL) to give the product as red crystals (75 mg, 69%). Anal. Calcd for $C_{67}H_{56}Cl_2N_2P_4Ru_2$ C, 62.57; H, 4.39; N, 2.18. Found: C, 56.79; H, 3.87; N, 1.92. ^{1}H NMR (CD_2Cl_2, 600 MHz): δ 4.11 (s, 5H, Cp), 4.93−5.03 (m, 4H, PCH_2P), 6.21 (d, 1H, H4), 7.17−7.26 (m, 16H, H_{ortho}), 7.31−7.38 (m, 8H, H_{para}), 7.40−7.55 (m, 18H, H_{meta}, H3′ and H5′), 7.67 (ddd, 1H, H4′), 7.77 (d, 1H, H3), 8.25 (s, 1H, H6), 9.53 (d, 1H, H6′). ^{13}C{^{1}H} NMR (CD_2Cl_2, 151 MHz): δ 49.8 (m, PCH_2P), 68.8 (s, Cp), 109.7 (s, C_β), 120.3 and 120.4 (s, C3 and C3′), 123.1 (s, C5′), 127.2 (m, C_{ortho}), 129.7 (m, C_{para}), 133.3 (m, C_{meta}), 134.2 (m, C_{ipso} and C5), 134.8 (s, C4′), 135.3 (s, C4), 144.0 (m, C_α), 148.3 (s, C6), 154.8 (s, C2), 156.0 (s, C6′), 156.3 (s, C2′). ^{31}P{^{1}H} NMR ($CDCl_3$, 243 MHz): −6.32 ppm (s). IR (CH_2Cl_2 solution): ν_{CC} 2048 cm^{-1}. MS (MALDI): m/z 1251 ([M − Cl]$^+$, 100%), 933 ([RuCl (CO)(dppm)$_2$]$^+$, 55%) 1283 ([M]$^+$, 10%), 910 ([RuCl(dppm)$_2$]$^+$, 10%). UV−vis (CH_2Cl_2) λ (nm) [$\varepsilon \times 10^4$ M^{-1} cm^{-1}]: 267 [4.09], 448 [1.72].

*[Ru{C≡Cbpy-κ^2-N′N-ReCl(CO)$_3$}Cl(dppm)$_2$] (**9**).* [Ru(C≡Cbpy)-Cl(dppm)$_2$] (50 mg, 0.046 mmol) and $ReCl(CO)_5$ (22 mg, 0.061 mmol) were dissolved in toluene (50 mL), and the solution was refluxed for 1 h, during which a bright yellow solution became deep red. The solvent volume was reduced to ca. 5 mL in vacuo, followed by the addition of hexane (25 mL) and cooling to 0 °C. The precipitate that formed was collected and washed with hexane (3 × 5 mL) to give the product as red crystals (59 mg, 90%). Crystals suitable for X-ray analysis were obtained through the slow evaporation of a CH_2Cl_2/hexane (1:1) solution of the complex under an inert atmosphere. Anal. Calcd for $C_{65}H_{51}Cl_2N_2O_3P_4ReRu{\cdot}3CH_2Cl_2$: C, 49.65; H, 3.49; N, 1.70. Found: C, 49.45; H, 3.41; N, 2.13. ^{1}H NMR (CD_2Cl_2, 600 MHz): δ 4.98 (m, 4H, PCH_2P), 6.47 (dd, 1H, H4), 7.18−7.32 (m, 16H, H_{meta}), 7.35−7.46 (m, 8H, H_{para}), 7.48−7.54 (m, 16H, H_{ortho}), 7.65 (ddd, 1H, H5′), 7.67 (ddd, 1H, H4′), 7.95 (ddd, 1H, H3′), 7.98 (dd, 1H, H3), 8.01 (dd, 1H, H6′), 8.93 (dd, 1H, H6). ^{13}C{^{1}H} NMR (CD_2Cl_2, 151 MHz): δ 49.6 (PCH_2P), 111.5 (s, C_β), 121.6 and 121.7 (C3 and C3′), 124.8 and 125.1 (C5 and C5′), 127.7 (C_{meta}), 129.6 (C_{para}), 132.8 (C_{ortho}), 133.5 (C_{ipso}), 138.2 and 138.4 (C4 and C4′), 146.6 (C2), 152.4 (s, C6′), 153.5 (s, $^2J_{CP}$ = 25.7 Hz, C_α), 154.0 (s, C6), 156.4 (C2′), 197.6 and 197.8 (CO). ^{31}P{^{1}H} NMR (CD_2Cl_2, 243 MHz): δ −6.99 (m). IR (CH_2Cl_2 solution): $\nu_{C\equiv C}$ 2049 cm^{-1}, $\nu_{C\equiv O}$ 2019 cm^{-1}, $\nu_{C\equiv O}$ 1915 cm^{-1}, and $\nu_{C\equiv O}$ 1894 cm^{-1}. MS (MALDI): m/z 933 ([RuCl(CO)(dppm)$_2$]$^+$, 100%), 910 ([RuCl(dppm)$_2$]$^+$, 75%), 1383 ([M]$^+$, 20%). UV−vis (CH_2Cl_2) λ (nm) [$\varepsilon \times 10^4$ M^{-1} cm^{-1}]: 261 [4.93], 325 [1.64], 480 [2.35].

*[RuCl(κ^2-N′N PhC$_2$bpy)Cp] (**10**).* PhC≡Cbpy (100 mg, 0.39 mmol) and [RuCl(COD)(Cp)] (115 mg, 0.37 mmol) were dissolved in acetone (20 mL), and the solution was stirred at room temperature for 20 h. The solvent volume was reduced to 10 mL *in vacuo*, and Et_2O (10 mL) was added before the mixture was cooled to 0 °C for 1 h. The precipitate that formed was collected and washed with Et_2O (2 × 3 mL) to give the product as a bright purple powder (128 mg, 75%). Crystals suitable for X-ray analysis were obtained through the vapor diffusion of *n*-pentane into a CH_2Cl_2 solution of the complex. Anal. Calcd for $C_{23}H_{17}ClN_2Ru$: C, 60.33; H, 3.74; N, 6.12. Found: C, 60.24; H, 3.96; N, 6.12. ^{1}H NMR (CD_2Cl_2, 500 MHz): δ 4.31 (s, 5H Cp), 7.28 (m, 1H, H5′), 7.18 (d, 1H, H4), 7.39−7.42 (m, 3H, H_{ortho} and H_{para}), 7.58 (m, 2H, H3 and H3′), 7.67 (ddd, 1H, H4′), 7.73 (dd, 1H, H4), 9.63 (dd, 1H, H6′), 9.77 (d, 1H, H6). ^{13}C{^{1}H} NMR (CD_2Cl_2, 126 MHz): δ 69.1 (Cp), 84.1 (C_β), 94.3 (C_α), 120.4 and 120.8 (C3 and C3′), 121.1 (C5), 121.3 (C_{ipso}), 123.9 (C5′), 127.7 (C_{ortho}), 128.5 (C_{para}), 131.0 (C_{meta}), 133.6 (C4′), 135.6 (C4), 153.5 (C2), 154.2 (C6′), 154.5 (C2′), 156.2 (C6). IR (KBr disk): $\nu_{C\equiv C}$ 2220 cm^{-1}. Mp ≥ 300 °C. MS (MeCN, ES (+)): m/z 464 ([Ru(NCMe)(PhC$_2$bpy)-Cp]$^+$, 100%), 458 ([M]$^+$, 15%). UV−vis (CH_2Cl_2) λ (nm) [$\varepsilon \times 10^4$ M^{-1} cm^{-1}]: 263 [2.98], 330 [7.97], 546 [0.69].

*[RuCl(κ^2-N′N-HC$_2$bpy)Cp] (**11**).* HC≡Cbpy (63 mg, 0.35 mmol) and [RuCl(COD)Cp] (101 mg, 0.33 mmol) were dissolved in acetone (15 mL), and the solution was stirred at room temperature for 22 h. The solvent volume was reduced to 5 mL *in vacuo* and cooled to 0 °C. The precipitate was collected and washed with Et_2O (2 × 10 mL) to give the product as a purple powder (102 mg, 82%). Anal. Calcd for $C_{17}H_{13}ClN_2Ru$: C, 53.48; H, 3.43; N, 7.34. Found: C, 53.33; H, 3.50; N, 7.24. ^{1}H NMR ($CDCl_3$, 500 MHz): δ 3.38 (s, 1H, C≡C*H*), 4.31 (s, 5H, Cp), 7.31 (m, 1H, H5′), 7.71−7.76 (m, 2H, H3′ and H4′), 7.92−7.97 (m, 2H, H4 and H3), 9.64 (dd, 1H H6′), 9.73 (s, 1H, H6). ^{13}C{^{1}H} NMR ($CDCl_3$, 126 MHz): δ 70.3 (*Cp*), 79.3 (C_β), 83.1 (C_α), 120.5 (C5), 121.2 (C3), 122.3 (C3′), 125.1 (C5′), 134.6 (C4′), 137.2 (C4), 155.3 (3 signals, C2, C2′, and C6′), 157.8 (C6). IR (KBr disk): $\nu_{C\equiv CH}$ 3133 cm^{-1}, $\nu_{C\equiv C}$ 2098 cm^{-1}. Mp ≥ 300 °C (dec). MS (MeCN, ES (+)): m/z 388 ([Ru(NCMe) (HC$_2$bpy)Cp]$^+$, 100%, 382 ([M]$^+$, 15%). UV−vis (CH_2Cl_2) λ (nm) [$\varepsilon \times 10^4$ M^{-1} cm^{-1}]: 259 [1.74], 313 [3.88], 367 [0.62], 538 [0.43].

*[ReCl(CO)$_3$(κ^2-N′N-PhC$_2$bpy)] (**12**).* PhC≡Cbpy (200 mg, 0.78 mmol) and [$ReCl(CO)_5$] (235 mg, 0.65 mmol) were dissolved in toluene (100 mL), and the solution was heated to reflux for 2 h, during which a colorless solution became bright yellow. The solvent volume was reduced to 20 mL *in vacuo*, and the mixture was cooled to 0 °C. The precipitate was collected on a filter and washed with EtOH (3 × 5 mL) to give the product as a yellow powder (285 mg, 78%). Anal. Calcd for $C_{21}H_{12}ClN_2O_3Re$: C, 44.88; H, 2.15; N, 4.98. Found: C, 45.12; H, 2.27; N, 4.81. ^{1}H NMR (CD_2Cl_2, 500 MHz): δ 7.41−7.47 (m, 3H, H_{ortho} and H5′), 7.56 (m, 1H, H_{para}), 7.62 (m, 2H, H_{meta}), 8.08−8.12 (m, 2H, H3′, and H4′), 8.15−8.19 (m, 2H, H3 and H4), 9.08 (dd, 1H, H6′), 9.16 (s, 1H H6). ^{13}C{^{1}H} NMR (CD_2Cl_2, 126 MHz): δ 84.1 (C_β), 97.8 (C_α), 121.8 (C_{ipso}), 123.1 and 123.9 (C3 and C3′), 124.7 (C5), 127.6 (C5′), 129.1 (C_{ortho}), 130.3 (C_{para}), 132.4 (C_{meta}), 139.6 (C4), 141.3 (C4′), 153.5 (C6′), 154.3 (C2), 155.5 (C6), 155.6 (C2′), 189.8 (CO), 197.8 (CO). IR (KBr disk): $\nu_{C\equiv C}$ 2222 cm^{-1}, $\nu_{C\equiv O}$ 2025 cm^{-1}, $\nu_{C\equiv O}$ 1914 cm^{-1}, and $\nu_{C\equiv O}$ 1894 cm^{-1}. Mp = 281−284 °C. MS (MeCN, ES (+)): m/z 644 ([M + 2 MeCN]$^+$, 20%), 601 ([M + MeCN]$^+$, 20%). UV−vis (CH_2Cl_2) λ (nm) [$\varepsilon \times 10^4$ M^{-1} cm^{-1}]: 255 [7.27], 344 [10.13].

*[ReCl(CO)$_3$(κ^2-N′N-HC$_2$bpy)] (**13**).*[38] [$ReCl(CO)_5$] (102 mg, 0.282 mmol) and HC≡Cbpy (60 mg, 0.33 mmol) were dissolved in toluene (40 mL). The solution was heated to reflux for 30 min during which the colorless solution turned deep red and then developed a yellow color along with the formation of a yellow precipitate. The yellow powder was collected and recrystallized from CH_2Cl_2/toluene to yield the product (98 mg, 0.20 mmol, 72%). Anal. Calcd for $C_{15}H_8ClN_2O_3Re{\cdot}0.75CH_2Cl_2$: C, 34.42; H, 1.74; N, 5.10%. Found: C, 34.26; H, 1.65; N, 5.47%. ^{1}H NMR ($CDCl_3$, 500 MHz): δ 3.53 (s, 1H, C≡CH), 7.57 (ddd, 1H, H5′), 8.08 (m, 2H, H3′ and H4′), 8.14 (dd, 1H, H4), 8.18 (dd, 1H, H4), 9.08 (ddd, 1H, H6′), 9.12 (dd, 1H, H6). ^{13}C{^{1}H} NMR ($CDCl_3$, 125.7 MHz): δ 77.7 (C_β), 85.7 (C_α), 122.4 (C3), 123.2 and 123.4 (C3′ and C5′), 127.4 (C5), 138.9 (C4′), 141.5 (C4), 153.4 (C2), 154.7 and 155.0 (C2′ and C6′), 155.8 (C6). IR (CH_2Cl_2, cm^{-1}): 2121 (w) ν(C≡C), 2024, 1922, and 1900 (vs) ν(CO). IR (Nujol): ν(*H*C≡C) 3185 (w) cm^{-1}. FAB+ MS: m/z 486 (45%, [M]$^+$), 450 (100%, [M-Cl]$^+$).

RESULTS AND DISCUSSION

Alkynyl Complexes. The cyclopentadienyl ruthenium alkynyl complexes **1** and **2** were prepared using well-trodden methodologies.[39,40] The syntheses of complexes **2**,[41] **3**,[27] and **13**[38] have been reported, but in the case of complex **2**, a more concise synthesis is reported here and a reinterpretation of the ^{13}C{^{1}H} NMR assignments is presented and supported with 2D NMR experiments, similarly with complex **13**. The X-ray crystal structures of **2** and **3** are presented here for the first time.

The bimetallic complexes were accessed through ligand substitution reactions on [RuCl(COD)Cp], for **4**, **6** and, **8** or [$ReCl(CO)_5$], for **5**, **7**, and **9**, in good yield. Similar reactions provided access to **10**−**13**, which are cogent examples for the comparison of physical and spectroscopic properties of **4**−**9**.

In the infrared spectra of the complexes the weak ν(C≡C) band of the free ligand (2097 cm^{-1}) shifted to a strong alkynyl stretch in the range 2038−2222 cm^{-1}, the majority lying in the

dx.doi.org/10.1021/om500172r | *Organometallics* 2014, 33, 4911−4922

range 2038−2070, for **1**−**9**, with bands for **10**−**13** between 2098 and 2222 cm^{-1}. Complexes **11** and **13** also displayed weak $\nu(\equiv C—H)$ bands for at 3122 and 3184 cm^{-1}, respectively. The binuclear complexes **4**−**9** had $\nu(C\equiv C)$ bands that were some ca. 30 cm^{-1} lower than those for the mononuclear **1**−**3**, the lower frequency attributed to a decrease of triple-bond character on account of withdrawal of electron density to the coordinated metal moiety at the bipyridyl nitrogens, and amplified by the increase in mass associated with the addition of the second metal unit. The $ReCl(CO)_3$ appended complexes, **5**, **7**, **9**, **12**, and **13**, all exhibit IR $\nu(CO)$ spectra characteristic of *fac* coordination of the of the CO ligands.

The proton NMR spectra contained the expected resonances for the cyclopentadienyl moieties with the methyl groups of the Cp* ligands at ca. 1.6 ppm. In the spectra of **2**, **4**, **6**−**8**, **10**, and **11**, signals for Cp were consistent with those normally observed for neutral ruthenium complexes and at ca. 4.4 ppm for Cp ligands attached to Ru(bisphospine) moieties and at ca. 4.1, for **4**, **6** and **8**, and at ca. 4.3 for **10** and **11** for those Cp ligands attached to Ru(bpy), notably the complex [RuCl(κ^2-*N*′*N*-bpy)Cp] has a resonance at 4.35 ppm for Cp in its ^1H NMR spectrum.[28,42] The alkynyl protons of **11** and **13** were observed as singlets at 3.38 and 3.53 ppm, respectively.

The $^{13}C\{^1H\}$ NMR spectra obtained for the complexes contained resonances that were diagnostic of the presence of an alkyne in all complexes. The revised assignment of the alkynyl carbons was achieved with the aid of 2-D HMBC experiments and the observation of coupling to the phosphorus nuclei, typically ca. 20 Hz. The C_α resonances were observed to be uniformly downfield of the C_β peaks for the alkynyl complexes were all identified with the C_α resonances all uniformly downfield of C_β, with the latter at ca. 110 ppm and the former in the range ca. 150−130 ppm. The $^{31}P\{^1H\}$-spectra contained singlets characteristic of the respective Ru(phosphine) moieties. Other resonances associated with the respective ligands were observed in the expected regions.

In an attempt to acquire microanalytical data for complex **8** we analyzed five different samples prepared from three different repeat reactions and have yet to get acceptable results. For this reason we have added copies of the characterization data (^1H, ^{13}C, and ^{31}P NMR and MALDI-TOF MS) to the Supporting Information that establish the absence of detectable contaminants.

Solid-State Structures. The structures of the alkynyl complexes **1**−**3** are depicted in Figure 1, with selected interatomic parameters collected in the Supporting Information (Tables S1, S3−S8). These tables also collect the data associated with the previously reported **2**[41] and **3**,[27] but for which no structures have been previously determined. We have previously published the structure of the dppe analogue of **3**, viz. [Ru(C≡Cbpy)Cl(dppe)$_2$].[27]

The bond lengths and angles about the {Ru(PPh$_3$)$_2$Cp} (**1**), {Ru(dppe)Cp*} (**2**), or {*trans*-RuCl(dppm)$_2$} (**3**) cores are unremarkable and consistent with other alkynyl complexes of this type, and the metal−C_2 parameters are also consistent with other metal−ligand systems. Here also the uncoordinated C≡Cbpy units in **1**−**3** are strictly comparable to the analogous units in other complexes containing this uncoordinated ligand.[27,38,43,44]

Crystals of **3**·toluene were mounted on a fiber under an atmosphere of cold CO_2 and transferred quickly to the cold stream to avoid any solvent loss. Some crystals were allowed to remain at room temperature for several days, after which they still appeared to still be crystalline. A second data set on these crystals, **3b** (Supporting Information) showed that, although they were still crystalline, the *b* cell length had decreased by about 12% with the other cell dimensions remaining almost unaltered. The decrease in the length of the crystal cell *b* parameter was clearly due to loss of the toluene solvent. The geometries of the molecules of the two complexes did not show any significant differences. The bimetallic complexes **5**−**7** and **9** also crystallized as solvates.

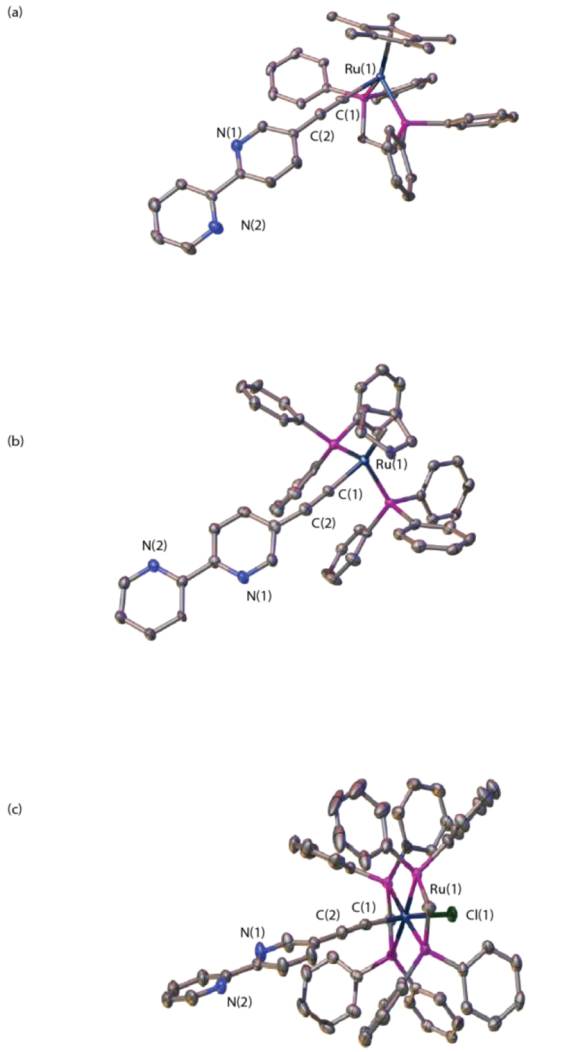

Figure 1. Molecular representations of the structures of (a) **1**, (b) **2** (one of the molecules), and (c) **3**. Hydrogen atoms omitted to aid in clarity. Atomic displacement envelopes shown at the 50% probability level.

The chloroform solvate molecule of **5**·$CHCl_3$ is closely associated with the Cp ring; the Me_5C_5 centroid···H−CCl_3 distance is 2.38 Å (Figure 2). These halocarbon H-bonds have been observed previously, notably in the supramolecular interactions of sarcophagine[45] complexes and metal calixarene complexes.[46−48] Hirshfeld surfaces, calculated using *CrystalExplorer 3.1*[49,50] provide a convenient method through which to investigate the nature of intermolecular interactions for many classes of complexes[51−55] and is well-suited to the analysis of the interactions in solvated structures. Using this approach, we find that the structure of **9** contains four CH_2Cl_2 molecules of solvation.

dx.doi.org/10.1021/om500172r | *Organometallics* 2014, 33, 4911−4922

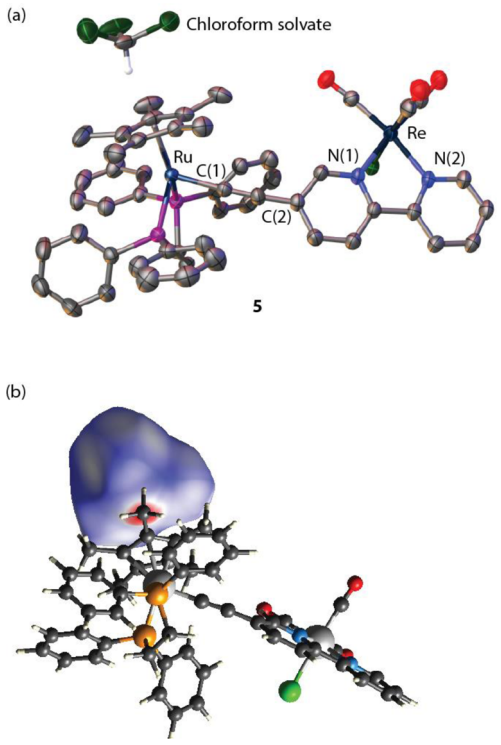

Figure 2. Molecular representations of the structure of complex **5** (a) showing the proximity of the solvate $CHCl_3$ to the Cp ring. Atomic displacement envelopes shown at 50% probability. (b) Hirshfeld surface of the solvate $CHCl_3$ in relation to **5**. The majority of hydrogen atoms omitted to aid in clarity in (a).

The structures of the bimetallic complexes **6**, **7**, and **9** are depicted in Figure 3. It is clear from the data in Tables S1 and S3−S8 (Supporting Information) that the coordination of a metal to the bipyridyl unit has had no significant effect on the length of the C≡C triple bond in any of the bimetallic complexes. Similarly, the structurally characterized, bipyridyl coordinated monometallic complexes **10** and **12** (Figure 4) and previously published **13** prepared for structural and spectroscopic comparisons show no appreciable differences in analogous distances. Clearly, the presence of the bpy ligated metal does not lead to any structurally significant differences in the formal valence bond representations, nor the evolution of any substantive degree of cumulenic character in the alkynyl linker.

To the best of our knowledge, there are no structurally characterized derivatives of the {Ru(bpy)Cp} moiety to allow comparison with **6** and **10**. Therefore, the known compound **15** was prepared and its structure determined crystallographically. In this model system, **15**, the distance of the Cp ring from the metal (as measured by the Ru−centroid distance, Ru−Cp′) is 1.78 Å (1.777−1.781 Å), which is about 0.1 Å shorter than that found in the $\{Ru(PPh_3)_2Cp\}$ core of **6**, and 0.6 Å shorter than that for $[RuCl(PPh_3)_2Cp]$.[S6] The Ru−Cl distance was around 2.45 Å (2.4475(3) to 2.4676(12) Å), which is consistent with other complexes. The binding of the bpy ligand was consistent across the three complexes **6**, **10**, and **15**, with Ru−N distances around 2.08 Å (2.0751(10) to 2.109(3) Å) and N−Ru−N bond angles of 76° (76.09 to 76.58). These bond lengths are slightly longer, with a narrower bond angle than seen in $[Ru(bpy)_3](PF_6)_2$ with a bond length of 2.056 Å and an angle of 78.7°.[S7]

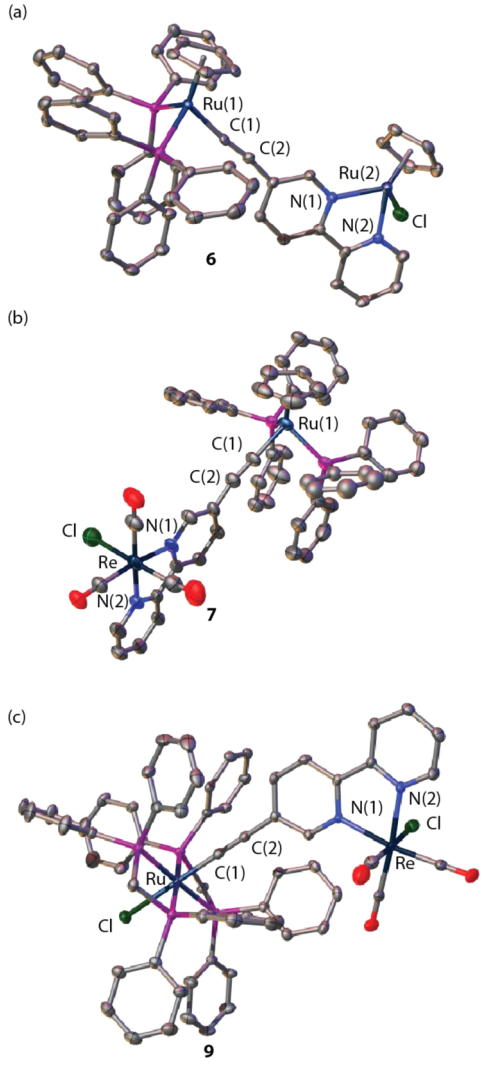

Figure 3. Molecular representations of the structures of (a) **6**, (b) **7**, and (c) **9**. Hydrogen atoms have been omitted to aid in clarity. Atomic displacement envelopes shown at 20% probability level.

There are two independent molecules of **12** in the asymmetric unit although of opposite chirality in the space group $P2_12_12_1$. Otherwise, the two molecules are similar, the difference being confined to minor orientations of the phenyl and bipyridyl rings. The dihedral angles between two pyridyl rings are 7.2(5) and 0.5(4)° for molecules 1 and 2 respectively. The dihedral angles between the phenyl ring and each of the bpyridyl rings are 2.3(5), 5.5(6)° for molecule 1 and 8.3(6) and 7.8(6)° for molecule 2.

The structure of ligand **14** was obtained, with three independent molecules in the structure. All three molecules are linear along the axis of the C≡C bond and have almost coplanar pyridine rings in the bpy moiety, with the nitrogen atoms in a transoid configuration and dihedral angles between the rings of 5.40(8), 4.85(8), and 8.42(8)°. In molecules 1 and 2, the phenyl rings are almost coplanar with the bipyridine moiety, with dihedral angles of 5.39(8) and 3.37(8)°, respectively, whereas in molecule 3, the phenyl ring is considerably rotated form the plane of the bpy moiety, with a dihedral angle of 40.35(8)°.

Electrochemistry. The redox properties of the monometallic complexes (**1**−**3**, **10**, **11**), bimetallic complexes (**4**−**9**),

dx.doi.org/10.1021/om500172r | *Organometallics* 2014, 33, 4911−4922

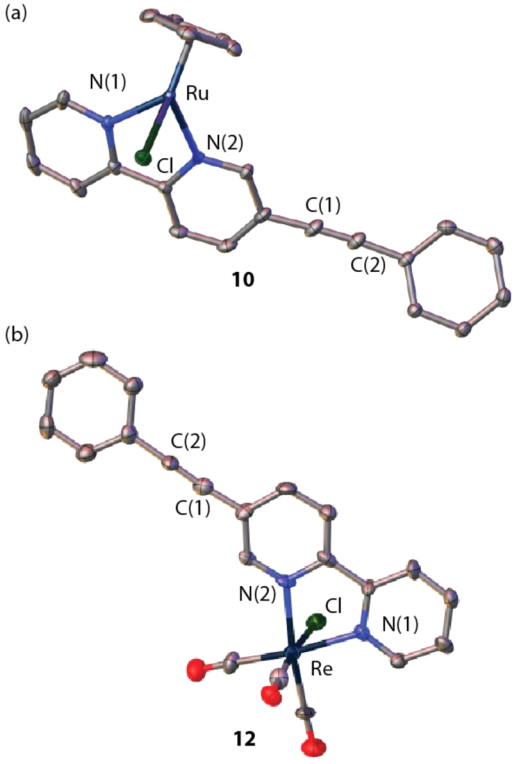

Figure 4. Molecular representations of the structures of (a) **10** and (b) **12** (one of the molecules). Hydrogen atoms omitted to aid in clarity. Atomic displacement envelopes shown at 50% probability.

and [RuCl(κ^2-*N*′*N*-bpy)Cp] (**15**) were measured by cyclic voltammetry, and relevant data are collected in Table 1.

Typically, ruthenium alkynyl complexes undergo one-electron oxidations to give the corresponding radical cations in which the unpaired electron is delocalized over the metal and alkynyl ligand. As a consequence, the redox potentials of ruthenium alkynyl complexes are a function of both the ligands

Table 1. Electrochemical Data for the Complexes 1−11 and 15[a]

	first oxid			second oxid			red.
compd	$E_{1/2}$ (V)	ΔE_p (mV)	I_a/I_c	$E_{1/2}$ (V)	ΔE_p (mV)	I_a/I_c	E_p (V)
1	0.00	77	1.09				
2	0.26	79	1.24				
3	0.14	73	1.09				
4	−0.16	76	1.10	0.09	74	1.58	
5	0.14	73	1.42				−1.91
6	−0.19	76	1.08	0.07	93	2.08	
7	0.40	79	2.55				−1.87
8	−0.16	83	1.04	0.26	119	1.21	
9	0.32	127	1.07				−1.95
10	0.07	113	0.99				
11	0.05	85	0.90				
15	−0.02	85	1.08				

[a] CH_2Cl_2 solutions containing 0.1 M $^nBu_4NPF_6$ electrolyte. The decamethylferrocene/decamethylferricenium ($FeCp^*_2/[FeCp^*_2]^+$) couple was used as an internal reference, with all potentials reported relative to the ferrocene/ferricenium couple ($FeCp_2/[FeCp_2]^+$ = 0 V, such that $FeCp^*_2/[FeCp^*_2]^+$ = −0.48 V in CH_2Cl_2).[58] Scan rate of 100 mV/s at room temperature.

on the ruthenium center and the alkynyl substituent.[17,59,60] The oxidations are apparently reversible or quasi-reversible with the ratio of peak currents being close to unity and anodic/cathodic wave separations (ΔE_p) between 70 and 130 mV, which compare with ΔE_p = 70 mV for the internal standards (ferrocene, $FeCp_2$, or decamethylferrocene, $FeCp^*_2$). In the case of **3** there is an additional anodic feature at ca. 0.35 V observed on the reverse scan that also exhibits a cathodic return wave at 0.30 V, which indicates an initial EC process.

Expectedly, the electron rich, Cp* derivative **1** is oxidized at the most negative potential of the monometallic alkynyl species **1**−**3**, whereas $E_{1/2}$ for the Ru$(PPh_3)_2$Cp analogue **2** is some 260 mV more positive. In contrast to the variation in redox potentials of **1**−**3**, the mononuclear Ru(bpy)Cp complexes **10**, **11**, and **15** all oxidize at ca. 0 V. Cyclic voltammograms of the ruthenium, binuclear complexes, **4**, **6**, **8** all exhibit two oxidation events the first of which fall near −0.2 V. Consideration of the relative potentials in Table 1 suggests the two redox processes in the bimetallic complexes **4**, **6**, and **8** can be approximated in terms of sequential oxidation of the {RuCl(bpy)Cp} and {Ru(C≡Cbpy)L_2Cp} fragments.

In contrast, the heterometallic binuclear complexes **5**, **7**, and **9** display greater variation in the first oxidation process, with $E_{1/2}$ falling between 0.14 for the {Ru(dppe)Cp*} complex **5** and 0.40 V for the {Ru$(PPh_3)_2$Cp} analogue **7**. In this case it is likely that the oxidation is centered on the metal−alkynyl moiety and shifted to more positive potentials by the effect of the electron withdrawing {ReCl$(CO)_3$(bpy)} fragment. These bimetallic complexes also contain an irreversible reduction event at ca. −2 V associated with the {ReCl$(CO)_3$(bpy)}.

Spectroelectrochemical Studies. IR and UV−vis−near IR spectroelectrochemical (SEC) investigations were undertaken to shed further illumination on the nature of these complexes, their redox chemistry and electronic structures.

The IR spectra of **1**−**3** each display a ν(C≡C) band near 2070 cm^{-1}, split by either the Fermi resonance[61,62] or the presence of different rotamers in solution.[63] Oxidation of complexes **1**−**3** results in the shift ν(C≡C) from ca. 2070 to ca. 1920 cm^{-1} (Figure 5) consistent with the formation of the ruthenium alkynyl radical cations $[\mathbf{1}-\mathbf{3}]^+$,[17,59,60] together with a second, presumably ν(C≡C) band near 2050 cm^{-1}, which was subsequently consumed on further oxidation. On reduction of each of $[\mathbf{1}-\mathbf{3}]^+$ the ν(C≡C) band associated with the neutral

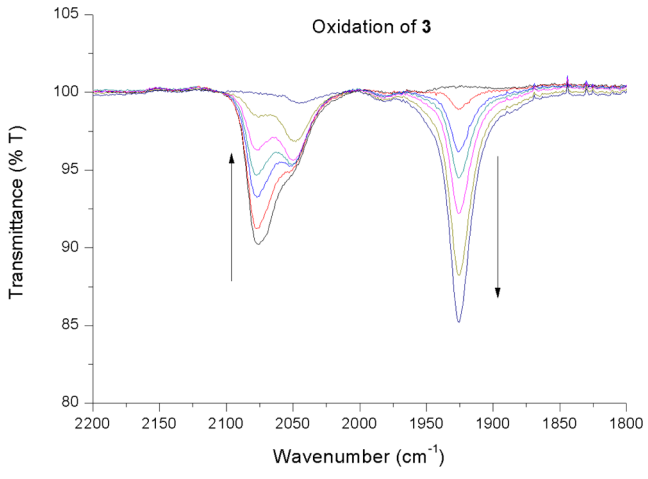

Figure 5. IR spectral changes accompanying the oxidation of complex **3** in an OTTLE cell, CH_2Cl_2 /0.1 M $^nBu_4NPF_6$ electrolyte.

dx.doi.org/10.1021/om500172r | *Organometallics* 2014, 33, 4911−4922

species at 2070 cm^{-1} is observed to grow back into the spectrum, together with the band at 2050 cm^{-1} of approximately equal intensity. The identity of these new species responsible for the persistent ν(C≡C) band at 2050 cm^{-1} is still undetermined. Initial theses revolved around the possibility of contamination but careful attention to detail in the collection of new data using rigorously purified materials discounted that possibility. Similarly, the possible ionization of the remaining halide in **3**, in the electrolyte used, giving rise to closely related alkynyl stretches in the IR spectrum was also discounted. The appearance of a similarly putative alkynyl band on oxidation was also observed in the IR SEC study of [Ru(C≡Cbpy)(dppe)Cp*] (**1**) and [Ru(C≡Cbpy)-$(PPh_3)_2$Cp] (**2**) where the formation of ionized products or solvent stabilized cations can be discounted.

It was posited that the new band is a result of a chemical process following the initial oxidation of the alkynyl complex on the relatively long time scale associated with the spectroelectrochemical study compared with the voltammetric measurements. Therefore, chemical oxidation of **1** using the acetylferrocenium ion in CH_2Cl_2 was performed to test the hypothesis. The reaction was monitored by IR spectroscopy and showed the formation of the radical alkynyl cation after some hours, evinced by the observation of a band at 1920 cm^{-1} and accompanied by a band for the unknown species at 2030 cm^{-1}. After 16 h, the radical alkynyl cation had decomposed to the carbonyl cation,[64,65] [Ru(CO)(dppe)Cp*]$^+$, giving a new band at 1972 cm^{-1}, with the band attributed to the unknown complex unchanged.

The nature of the species present in the solution was probed by mass spectrometry and analysis of the spectra obtained was inconclusive, apart from expected daughter ions related to the [Ru(dppe)Cp*]$^+$ core and ions related to the carbonyl cation. However, there was a doubly charged ion observed at 1249 *m/2z*, which displayed a characteristic Ru_2 isotope pattern that led us to suggest that the oxidation of **3** led to some oligomerization of the alkynyl radical cation complex, most likely dimerization. Oxidation of alkynyl complexes leading to oligiomerisation was demonstrated in many systems,[66−69] and the noninnocent nature of ligands in redox reactions was highlighted by one of us recently.[60]

The IR SEC study of the ruthenium, binuclear complexes, **4**, **6**, and **8**, (illustrated for **8** in Figure 6) shows that there is a slight shift ($\Delta\nu$(C≡C): **4**/[**4**]$^+$ −9 ; [**6**]/[**6**]$^+$ −9; **8**/[**8**]$^+$ −5 cm^{-1}) to lower wavenumber of the ν(C≡C) band on the first oxidation of the complex, consistent with initial oxidation localized on the {RuCl(bpy)Cp} moiety and therefore not significantly affecting the triple bond character of the alkynyl complex. However, on further oxidation to the dication the ν(C≡C) band loses intensity, becoming almost indistinguishable from the baseline in the case of [**4**]$^{2+}$ and [**6**]$^{2+}$, which suggests a limited dipole over the alkynyl moiety and shifts to lower frequency; both observations are consistent with the second oxidation being more associated with the {Ru-$(PPh_3)_2$Cp} fragment. However, in the case of **8**, the ν(C≡C) band has enough intensity to be observed at 1947 cm^{-1} but is significantly less intense than the neutral species. This feature is found to be reversible on reduction under the conditions of the spectroelectrochemical measurements.

The heterometallic binuclear complexes, **5**, **7**, and **9** all displayed consistent IR SEC behavior, illustrated here by complex **9** (Figure 7). Oxidation occurs at the Ru alkynyl substituent, resulting in the typical shift in ν(C≡C) frequency

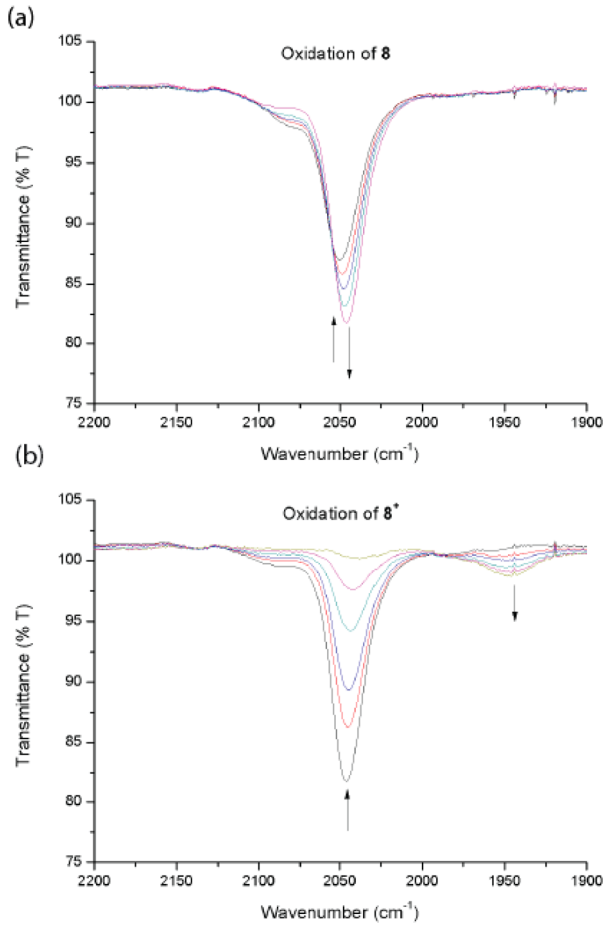

Figure 6. IR spectral changes accompanying the oxidation of complex (a) **8** to [**8**]$^+$ and (b) [**8**]$^+$ to [**8**]$^{2+}$ in an OTTLE cell, CH_2Cl_2 /0.1 M $^nBu_4NPF_6$ electrolyte.

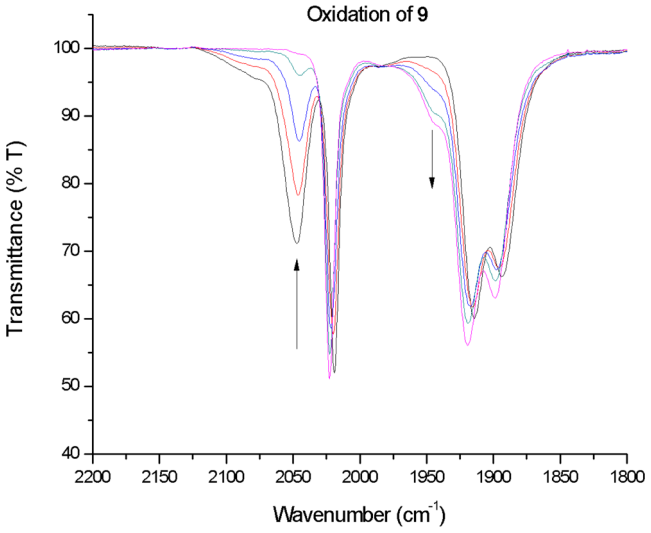

Figure 7. IR spectral changes accompanying the oxidation of complex **9** in an OTTLE cell, CH_2Cl_2 /0.1 M $^nBu_4NPF_6$ electrolyte.

to lower energy and causing it to be largely obscured by the ν(CO) bands associated with the {$Re(CO)_3$(bpy)} fragment, which change little in intensity or position. The shoulder at 1940 cm^{-1} in [**9**]$^+$ likely arises from the incomplete obstruction of the ν(CC) stretch.

dx.doi.org/10.1021/om500172r | *Organometallics* 2014, 33, 4911−4922

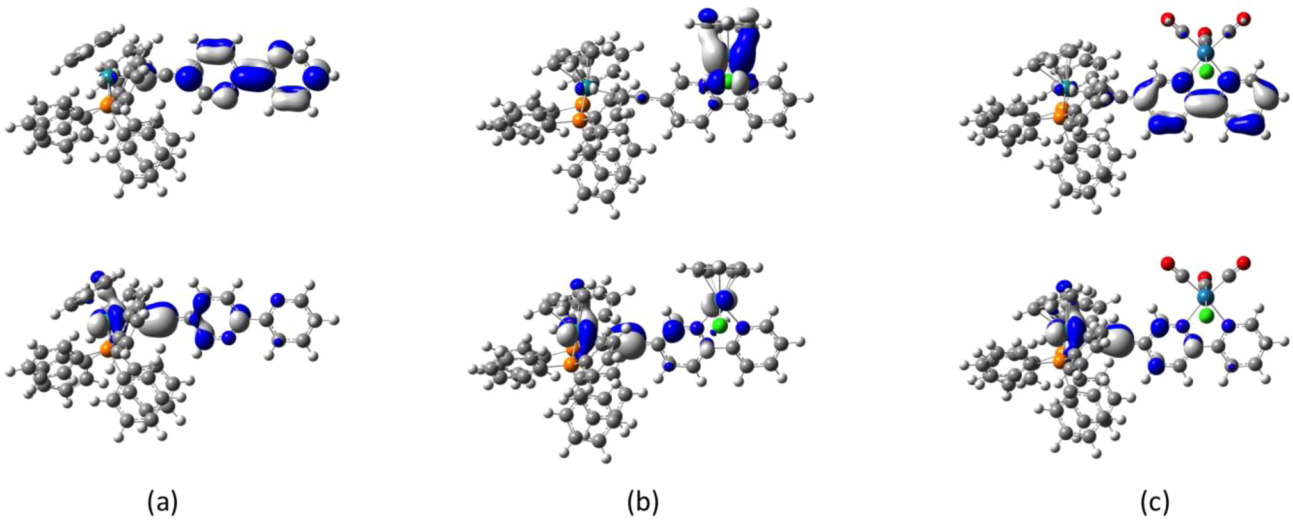

Figure 8. Plots of selected molecular orbitals (isocontour value ±0.04 (e/bohr^3)$^{1/2}$): (a) the LUMO (top) and HOMO (bottom) of **2′**; (b) the HOMO and HOMO−1 of **6′**; (c) the LUMO (top) and HOMO (bottom) of **7′**.

The bimetallic complexes **4**−**9** were further investigated by UV−vis−NIR spectroelectrochemical studies, seeking any additional evidence for interactions between the metallic centers mediated by the ethynyl bipyridyl bridging moiety. The homobimetallic ruthenium complexes **4**, **6**, and **8** all exhibit similar spectroscopic profiles, with the MLCT transitions associated with the ruthenium−alkynyl fragment observed near ca. 450 nm. On oxidation, these bands are only slightly red-shifted to ca. 500 nm, together with a very low intensity IVCT band near 1200 nm (8300 cm^{-1}). These trends are consistent with the initial oxidation of the {RuCl(bpy)Cp} fragment, which leads to an inductive stabilization of the bpy ligand π^*-system and hence lowering in the MLCT transition energy. Further oxidation to the dications $[\mathbf{4}]^{2+}$, $[\mathbf{6}]^{2+}$, and $[\mathbf{8}]^{2+}$ causes a collapse in the lowest energy feature, consistent with the IVCT assignment, and the 500 nm band, with new bands at ca. 700−800 nm and a characteristic blue shift in the MLCT band consistent with the greater degree of Ru—C≡C character in the second oxidation event. In addition, in the case of $[\mathbf{8}]^{2+}$ a Cl → {RuC≡C}$^+$ LMCT transition, which is significantly narrower and more intense than the IVCT band, is also observed at 1280 nm (7800 cm^{-1}).[63]

Further investigation of the heterobimetallic Ru−Re complexes using UV−vis−NIR spectroelectrochemical methods also supports these assignments. In the case of **5**, **7**, and **9**, the only accessible oxidation process causes a blue shift in the ruthenium−alkynyl MLCT band. For $[\mathbf{5}]^+$, the dπ−dπ transition often associated with [Ru(C≡CR)(L$_2$)Cp′]$^+$ radical cations was observed clearly near 1500 nm (6650 cm^{-1}),[59] with a Re → {Ru(C≡CR)}$^+$ CT band observed near 730 nm (13,700 cm^{-1}), similar processes being known for related Re/Fe complexes.[70,71]

Similar transitions are apparent on close inspection of the spectrum of the Ru(PPh$_3$)$_2$Cp derivative $[\mathbf{7}]^+$, although these features are rather less pronounced. The spectrum of $[\mathbf{9}]^+$ also features low energy transitions at 1230 and 860 nm, assigned to Cl → {RuC≡C}$^+$ LMCT and Re → {Ru(C≡CR)}$^+$ CT bands. As oxidation proceeds, other features at 990, 640, 383, and 356 nm grow in, accompanied by a loss of isosbestic points and indicating a degree of decomposition of the sample over the time scale of the spectroelectrochemical experiment.

Computational Studies. To aid in the interpretation of the electrochemical and spectroelectrochemical results, and to arrive at a more comprehensive description of the electronic structure of the complexes described here, a series of DFT calculations (B3LYP/LANL2DZ Ru and Re/6-31G** all other atoms/CPCM−dichloromethane solvent model) were carried out on the representative series $[\mathbf{2}']^{n+}$ (n = 0, 1), $[\mathbf{6}']^{n+}$ (n = 0, 1, 2), and $[\mathbf{7}']^{n+}$ (n = 0, 1), where the prime (′) notation is used to distinguish the computational systems from the physical samples.

Optimized bond lengths and angles from **2′**, **6′**, and **7′** were in good agreement with those of the crystallographically determined structures (Tables S3−8, Supporting Information) with overestimation of the Ru−P, Ru−Cl, and Re−Cl, and Ru−Cp′ bond lengths by ca. 4%. Calculated vibrational frequencies (scaled here by 0.95),[72] particularly the ν(C≡C) and ν(CO) modes, provide an excellent point for comparison of the model and physical systems in the various electrochemically accessible redox states (Table 1), and the close agreement between these data give confidence in the conclusions drawn from the computational work.

Compound **2′** is another member in the now well-studied family of complexes Ru(C≡CR)(PR$_3$)$_2$Cp′,[59,73−75] and the electronic structure is, not surprisingly, similar to the many other examples of this family described earlier at various levels of theory. Of the various minima of **2′** that can be identified, differing in the relative orientations of the N atoms relative to the Ru(PPh$_3$)$_2$Cp fragment and each other, the one represented by the structure depicted in Chart 1, with the bpy plane approximately bisecting the P−Ru−P angle, is the global minimum. The analogous structure with the bpy fragment oriented as found in the crystallographically determined structure lies some 2.3 kJ mol^{-1} eV higher in energy.

The HOMO is distributed over the Ru—C≡C—bpy backbone (Ru 33%, C≡C 29%, bpy 24%) whereas at the level of theory employed the LUMO is essentially (88%) composed of the bpy π^* system, Figure 8. In comparison with **2′**, the 17-e compound $[\mathbf{2}']^+$ offers the usual pattern of elongated Ru—P and Ru—Cp′ bond lengths, which reflects decreases in metal—ligand π-back-bonding. The shorter Ru—C1 and C2—C3 bond lengths and longer C1—C2 bond in

dx.doi.org/10.1021/om500172r | Organometallics 2014, 33, 4911−4922

$[\mathbf{2}']^+$ are consistent with the composition and nodal structure of the β-LUSO (Ru 38%, C≡C 26%, bpy 21%), which has obvious similarities with the HOMO of **2**. The calculated ν(C≡C) frequencies in **2**′ and $[\mathbf{2}']^+$ track the geometric changes and orbital structure, decreasing from 2034 cm^{-1} (**2**′) to 1922 cm^{-1} ($[\mathbf{2}']^+$) as the C≡C character decreases on oxidation, in very good agreement with the IR spectroelectrochemical results. The substantial ethynylbipyridine ligand character in the radical cation $[\mathbf{2}']^+$ also supports the notion of interligand coupling proposed above to explain the chemical behavior of the closely related complexes $[\mathbf{1}-\mathbf{3}]^+$.

The electronic structure of bimetallic **6**′ allows some useful comparisons of phosphine and bpy ligated $RuXL_2Cp$ fragments,[28,76,77] a comparison that has additional relevance given the extensive knowledge of $RuX(PR_3)_2Cp'$ chemistry, and recent proposals for water oxidation catalysts based on the less well explored {Ru(bpy)Cp′} moiety.[78] The coordination of the RuClCp fragment to the bpy moiety in **2**′ has no discernible structural effect on the Ru(C≡Cbpy)$(PPh_3)_2$Cp fragment, whereas the various bond lengths and angles in the RuCl(bpy)Cp fragment in **6**′ are similar to those observed crystallographically for **10**. Perhaps of greatest interest is the contraction of the Ru—Cp′ bond length in the bpy coordinated fragment vs the phosphine coordinated fragments, which arises from the extremely efficient σ-donor properties of the bpy ligand and increased Ru—Cp back-bonding. This back-bonding contribution is reflected in the structure of the HOMO of **6**′, which is localized on the RuCl(bpy)Cp fragment (Ru2 62%, Cp 14%). The Ru—C≡C—bpy moiety that comprises the HOMO of **2**′ features heavily in the HOMO−1 of **6**′ (Ru1 31%, C≡C 23%, bpy 16%), which lies some 0.18 eV lower in energy than the HOMO, Figure 8. The local coordinates most appropriate for describing the two $RuXL_2Cp$ fragments are approximately orthogonal (Ru1—C1—Ru2—Cl 99.99°), and consequently there is little mixing between the metal-based orbitals through the ethynyl-bipyridyl bridge.

The cation radical $[\mathbf{6}']^+$ features bond lengths at the Ru(C≡Cbpy)$(PPh_3)_2$Cp fragment that are essentially unchanged from those of **6**′ and **2**′. In contrast, there is a modest (0.01−0.02 Å) contraction of the Ru2—N bond lengths, and a more significant shortening of the Ru2—Cl bond (reflecting a greater electrostatic attraction between the formally d^5, Ru^{III} center, and the Cl atom) and elongation of the Ru2—Cp′ distance as the metal—ring back-bonding interactions are diminished. The orthogonal relationship between the HOMO and HOMO−1 and localization on each of the two $RuXL_2Cp$ fragments is also evident in $[\mathbf{6}']^+$. On the basis of the structural characteristics and the distribution of the β-HOSO (Ru1 40%, C≡C 25%, bpy 17%) and β-LUSO (Ru2 60%, Cp2 13%, Cl 10%) in $[\mathbf{6}']^+$ and the observation of a low intensity IVCT band in each of $[\mathbf{4}]^+$, $[\mathbf{6}]^+$, and $[\mathbf{8}]^+$ (vide supra) these bis(ruthenium) radical cations can be accurately described as weakly coupled, or Class II, d^5/d^6 mixed-valence complexes. This localized electronic structure description is entirely consistent with the IR spectroelectrochemical observations, with the limited shift in the ν(C≡C) frequency between **6** and $[\mathbf{6}]^+$ ($\Delta\nu$(C≡C) = −8 cm^{-1}) mirrored in the models **6**′ and $[\mathbf{6}']^+$ ($\Delta\nu$(C≡C) = −16 cm^{-1}).

Although $[\mathbf{6}]^{2+}$ proved to be unstable under the conditions of the spectroelectrochemical experiment, the localization of the β-LUSO and β-HOSO on the RuCl(bpy)Cp and RuC≡Cbpy fragments in $[\mathbf{6}']^+$, respectively, is consistent with the interpretation of the cyclic voltammogram of **6** in terms of sequential oxidation of the RuCl(bpy)Cp and RuC≡Cbpy moieties.

Finally, turning attention to the mixed-metal complexes, **7**′ and $[\mathbf{7}']^+$ successfully modeled both the geometric properties of the crystallographically determined structure of **7** (Tables S3 and S7, Supporting Information) and the ν(C≡C) and ν(CO) frequencies from the IR spectroelectrochemical experiments (Table S10, Supporting Information). Importantly, the ν(C≡C) band in **7**′ (2020 cm^{-1}), which is well removed from the three ν(CO) bands (1979, 1878, 1864 cm^{-1}) shifts by some −94 cm^{-1} in $[\mathbf{7}']^+$ and falls within the ν(CO) bands, which are only modestly shifted to higher wavenumbers (ν(C≡C) 1926 cm^{-1}; ν(CO) 1984, 1887, 1872 cm^{-1}). Clearly, oxidation of **7** is associated with changes in the electron density in the RuC≡Cbpy moiety, which is reflected in the orbital structures of **7**′ and $[\mathbf{7}']^+$, Figure 8. Unsurprisingly, the HOMO of **7**′ displays the familiar RuC≡Cbpy character and nodal properties (Ru 37%, C≡C26%, bpy 20%) associated with the HOMO of **2**′ and the HOMO−1 of **6**′. Other Ru$(PPh_3)_2$Cp based orbitals contribute to the HOMO−1 and HOMO−2. The ReCl$(CO)_3$(bpy) fragment contributes mixed Re—Cl orbitals to the HOMO−3 and HOMO−4, which lie ca. 1 eV below the HOMO, whereas the LUMO is heavily bpy π^* in character (84%). In $[\mathbf{7}']^+$ the β-LUSO retains similar RuC≡Cbpy character (Ru 42%, C≡C 22%, bpy 19%) consistent with oxidation at this metal−organic fragment. This leads to a degree of orbital reordering, with stabilization of the occupied β-orbitals localized on the Ru$(PPh_3)_2$Cp fragment that now lies below the ReCl based fragment orbitals, supporting the assignment of the Re → {Ru(C≡CR)}$^+$ CT bands observed in the spectroelectrochemical experiments.

■ CONCLUSIONS

Some new bipyridyl appended ruthenium alkynyl complexes have been prepared, and these have allowed access to a range of binuclear homometallic ruthenium and heterometallic ruthenium−rhenium complexes. The coordination of a second metal center to the alkynyl complexes has little impact on the structures of these complexes except that imposed by the packing of these into the crystal lattice.

In the bimetallic complexes, the IR and UV−vis spectroelectrochemical experiments showed the two metal centers were found to be only weakly coupled, as evinced and supported by quantum chemical calculations. The alkynyl complexes of the type [Ru(C≡Cbpy){L_n}] ({L_n} = {$(PPh_3)_2$Cp}, {(dppe)Cp*}, {$Cl(dppm)_2$}) undergo reversible one-electron oxidations centered largely on the alkynyl ligands as has been observed previously for closely related complexes.

The homometallic binuclear complexes, represented by [Ru(C_2bpy-κ^2-$N'N$-RuClCp)$(PPh_3)_2$Cp] undergo two essentially reversible oxidations, the first centered on the (C_2bpy-κ^2-$N'N$-RuClCp) moiety and the second on the Ru(C≡Cbpy)$(PPh_3)_2$Cp fragment, leading to radical cations that can be described as Class II mixed-valence complexes. The heterometallic binuclear complexes [Ru(C_2bpy-κ^2-$N'N$-ReCl$(CO)_3$){L_n}] display a similar behavior, with initial oxidation on the ruthenium fragment giving rise to a new optical absorption band with Re → Ru(C≡Cbpy) charge transfer character. The heterometallic complexes also exhibit irreversible reductions associated with the Re hetereocycle moiety.

In summary, we have investigated the electronic structure of the bimetallic compounds prepared by us.

dx.doi.org/10.1021/om500172r | Organometallics 2014, 33, 4911−4922

■ ASSOCIATED CONTENT

Supporting Information

Cyclic voltammograms, IR spectra, and UV−vis−near-IR spectra of complexes during oxidation in a spectroelectrochemical cell. Tables of crystallographic data, bond lengths, and bond angles. ^{1}H, ^{13}C, and ^{31}P NMR and MALDI-TOF MS spectra for complex **8**. Cartesian coordinates of all optimised geometries as a .mol file. Table of observed and calculated vibrational frequencies. Cartesian coordinates. Tables of energy and composition data. CIF and Checkcif files for compounds **1**−**3**, **9**, **10**, and **12**−**15** (CCDC 980469−980478) and **5**−**7** (CCDC 986580−986582). This material is available free of charge via the Internet at http://pubs.acs.org.

■ AUTHOR INFORMATION

Corresponding Authors

*G. Koutsantonis. E-mail: george.koutsantonis@uwa.edu.au.
*P. J. Low. E-mail: paul.low@uwa.edu.au.

Author Contributions

C.F.R.M. performed all of the synthetic experimental work reported in this paper. B.W.S. and D.S.Y. are responsible for the crystallographic content. All authors contributed to the writing of this manuscript. All authors approve of the final version of the manuscript.

Notes

The authors declare no competing financial interest.

■ ACKNOWLEDGMENTS

This work was supported in part by the Danish National Research Foundation (DNRF93) Center for Materials Crystallography. We acknowledge the Diamond Light Source for an award of instrument time on the Station I19 (MT 6749) and the instrument scientists for support. The authors acknowledge the facilities and the scientific and technical assistance of the Australian Microscopy and Microanalysis Research Facility at the Centre for Microscopy, Characterisation and Analysis, The University of Western Australia, a facility funded by the University, State and Commonwealth Governments. P.J.L. gratefully acknowledges support from the Australian Research Council (FT120100073). C.F.R.M. was the holder of an Australian Postgraduate Award.

■ REFERENCES

(1) Diehl, M. R.; Steuerman, D. W.; Tseng, H.-R.; Vignon, S. A.; Star, A.; Celestre, P. C.; Stoddart, J. F.; Heath, J. R. *ChemPhysChem* **2003**, *4*, 1335.
(2) Joachim, C.; Gimzewski, J. K.; Aviram, A. *Nature* **2000**, *408*, 541.
(3) Kwok, K. S.; Ellenbogen, J. C. *Mater. Today* **2002**, *5*, 28.
(4) Lindsay, S. *Faraday Discuss.* **2006**, *131*, 403.
(5) Petty, M. In *Springer Handbook of Electronic and Photonic Materials*; Kasap, S., Capper, P., Eds.; Springer: New York, 2006; p 1219.
(6) Reimers, J. R.; Bilić, A.; Cai, Z.-L.; Dahlbom, M.; Lambropoulos, N. A.; Solomon, G. C.; Crossley, M. J.; Hush, N. S. *Aust. J. Chem.* **2004**, *57*, 1133.
(7) Tour, J. M. *Acc. Chem. Res.* **2000**, *33*, 791.
(8) Liang, W.; Shores, M.; Bockrath, M.; Long, J.; Park, H. *Nature* **2002**, *417*, 725.
(9) Park, J.; Pasupathy, A. N.; Goldsmith, J. I.; Chang, C.; Yaish, Y.; Petta, J. R.; Rinkoski, M.; Sethna, J. P.; Abruna, H. D.; McEuen, P. L.; Ralph, D. C. *Nature* **2002**, *417*, 722.
(10) Costuas, K.; Rigaut, S. *Dalton Trans.* **2011**, *40*, 5643.
(11) D'Alessandro, D. M.; Keene, F. R. *Chem. Soc. Rev.* **2006**, *35*, 424.
(12) Malvolti, F.; Rouxel, C.; Mongin, O.; Hapiot, P.; Toupet, L.; Blanchard-Desce, M.; Paul, F. *Dalton Trans.* **2011**, *40*, 6616.
(13) Akita, M.; Koike, T. *Dalton Trans.* **2008**, 3523.
(14) Bruce, M. I.; Low, P. J. *Adv. Organomet. Chem.* **2004**, *50*, 179.
(15) Dembinski, R.; Bartik, T.; Bartik, B.; Jaeger, M.; Gladysz, J. A. *J. Am. Chem. Soc.* **2000**, *122*, 810.
(16) Paul, F.; Lapinte, C. *Coord. Chem. Rev.* **1998**, *178*−*180*, 431.
(17) Low, P. J. *Coord. Chem. Rev.* **2013**, *257*, 1507.
(18) Wang, C. S.; Batsanov, A. S.; Bryce, M. R.; Martin, S.; Nichols, R. J.; Higgins, S. J.; Garcia-Suarez, V. M.; Lambert, C. J. *J. Am. Chem. Soc.* **2009**, *131*, 15647.
(19) Haiss, W.; Wang, C. S.; Grace, I.; Batsanov, A. S.; Schiffrin, D. J.; Higgins, S. J.; Bryce, M. R.; Lambert, C. J.; Nichols, R. J. *Nat. Mater.* **2006**, *5*, 995.
(20) Kaliginedi, V.; Moreno-Garcia, P.; Valkenier, H.; Hong, W. J.; Garcia-Suarez, V. M.; Buiter, P.; Otten, J. L. H.; Hummelen, J. C.; Lambert, C. J.; Wandlowski, T. *J. Am. Chem. Soc.* **2012**, *134*, 5262.
(21) Marques-Gonzalez, S.; Yufit, D. S.; Howard, J. A. K.; Martin, S.; Osorio, H. M.; Garcia-Suarez, V. M.; Nichols, R. J.; Higgins, S. J.; Cea, P.; Low, P. J. *Dalton Trans.* **2013**, *42*, 338.
(22) Moreno-Garcia, P.; Gulcur, M.; Manrique, D. Z.; Pope, T.; Hong, W.; Kaliginedi, V.; Huang, C.; Batsanov, A. S.; Bryce, M. R.; Lambert, C.; Wandlowski, T. *J. Am. Chem. Soc.* **2013**, *135*, 12228.
(23) Rigaut, S. *Dalton Trans.* **2013**, *42*, 15859.
(24) Packheiser, R.; Lang, H. *Inorg. Chem. Commun.* **2007**, *10*, 580.
(25) Packheiser, R.; Ecorchard, P.; Rueffer, T.; Lang, H. *Chem.—Eur. J.* **2008**, *14*, 4948.
(26) Armarego, W. L. F.; Chai, C. L. L. *Purification of Laboratory Chemicals* (Sixth ed.); Butterworth-Heinemann: Oxford, 2009.
(27) Koutsantonis, G. A.; Jenkins, G. I.; Schauer, P. A.; Szczepaniak, B.; Skelton, B. W.; Tan, C.; White, A. H. *Organometallics* **2009**, *28*, 2195.
(28) Albers, M. O.; Robinson, D. J.; Singleton, E. *J. Organomet. Chem.* **1986**, *311*, 207.
(29) Bruce, M. I.; Corbin, P. E.; Humphrey, P. A.; Koutsantonis, G. A.; Liddell, M. J.; Tiekink, E. R. T. *J. Chem. Soc., Chem. Commun.* **1990**, 674.
(30) Bruce, M. I.; Ellis, B. G.; Low, P. J.; Skelton, B. W.; White, A. H. *Organometallics* **2003**, *22*, 3184.
(31) Packheiser, R.; Ecorchard, P.; Rüffer, T.; Walfort, B.; Lang, H. *Eur. J. Inorg. Chem.* **2008**, 4152.
(32) Grosshenny, V.; Romero, F. M.; Ziessel, R. *J. Org. Chem.* **1997**, *62*, 1491.
(33) Schwab, P. F. H.; Fleischer, F.; Michl, J. *J. Org. Chem.* **2002**, 443.
(34) Pautzsch, T.; Rode, C.; Klemm, E. *J. Prakt. Chemie* **1999**, *341*, 548.
(35) Krejcik, M.; Danek, M.; Hartl, F. *J. Electroanal. Chem. Interfacial Electrochem.* **1991**, *317*, 179.
(36) Sheldrick, G. M. *Acta Crystallogr.* **2008**, *A64*, 112.
(37) Dolomanov, O. V.; Bourhis, L. J.; Gildea, R. J.; Howard, J. A. K.; Puschmann, H. *J. Appl. Crystallogr.* **2009**, *42*, 339.
(38) Packheiser, R.; Jakob, A.; Ecorchard, P.; Walfort, B.; Lang, H. *Organometallics* **2008**, *27*, 1214.
(39) Bruce, M. I.; Koutsantonis, G. A. *Aust. J. Chem.* **1991**, *44*, 207.
(40) Bruce, M. I.; Koutsantonis, G. A.; Liddell, M. J.; Nicholson, B. K. *J. Organomet. Chem.* **1987**, *320*, 217.
(41) Packheiser, R.; Ecorchard, P.; Walfort, B.; Lang, H. *J. Organomet. Chem.* **2008**, *693*, 933.
(42) Perekalin, D. S.; Karslyan, E. E.; Trifonova, E. A.; Konovalov, A. I.; Loskutova, N. L.; Nelyubina, Y. V.; Kudinov, A. R. *Eur. J. Inorg. Chem.* **2013**, *2013*, 481.
(43) Vicente, J.; Gil-Rubio, J.; Barquero, N.; Jones, P. G.; Bautista, D. *Organometallics* **2008**, *27*, 646.
(44) Packheiser, R.; Jakob, A.; Ecorchard, P.; Walfort, B.; Lang, H. *Organometallics* **2008**, *27*, 1214.
(45) Clark, I. J.; Crispini, A.; Donnelly, P. S.; Engelhardt, L. M.; Harrowfield, J. M.; Jeong, S.-H.; Kim, Y.; Koutsantonis, G. A.; Lee, Y. H.; Lengkeek, N. A.; Mocerino, M.; Nealon, G. L.; Ogden, M. I.; Park, Y. C.; Pettinari, C.; Polanzan, L.; Rukmini, E.; Sargeson, A. M.;

Skelton, B. W.; Sobolev, A. N.; Thuery, P.; White, A. H. *Aust. J. Chem.* **2009**, *62*, 1246.
(46) Bilyk, A.; Dunlop, J. W.; Hall, A. K.; Harrowfield, J. M.; Hosseini, M. W.; Koutsantonis, G. A.; Skelton, B. W.; White, A. H. *Eur. J. Inorg. Chem.* **2010**, 2089.
(47) Bilyk, A.; Dunlop, J. W.; Fuller, R. O.; Hall, A. K.; Harrowfield, J. M.; Hosseini, M. W.; Koutsantonis, G. A.; Murray, I. W.; Skelton, B. W.; Stamps, R. L.; White, A. H. *Eur. J. Inorg. Chem.* **2010**, 2106.
(48) Bilyk, A.; Dunlop, J. W.; Fuller, R. O.; Hall, A. K.; Harrowfield, J. M.; Hosseini, M. W.; Koutsantonis, G. A.; Murray, I. W.; Skelton, B. W.; Sobolev, A. N.; Stamps, R. L.; White, A. H. *Eur. J. Inorg. Chem.* **2010**, 2127.
(49) Spackman, M. A.; Jayatilaka, D. *CrystEngComm* **2009**, *11*, 19.
(50) Wolff, S. K.; Grimwood, D. J.; McKinnon, J. J.; Turner, M. J.; Jayatilaka, D.; Spackman, M.A. *CrystalExplorer 3.1*; University of Western Australia, 2010.
(51) Wright, P. J.; Muzzioli, S.; Skelton, B. W.; Raiteri, P.; Lee, J.; Koutsantonis, G.; Silvester, D. S.; Stagni, S.; Massi, M. *Dalton Trans.* **2013**, *42*, 8188.
(52) Fuller, R. O.; Griffith, C. S.; Koutsantonis, G. A.; Lapere, K. M.; Skelton, B. W.; Spackman, M. A.; White, A. H.; Wild, D. A. *CrystEngComm* **2012**, *14*, 804.
(53) Lee, J. J.; Fuller, R. O.; Sobolev, A. N.; Clausen, H. F.; Overgaard, J.; Koutsantonis, G. A.; Iversen, B. B.; Spackman, M. A. *Chem. Commun.* **2011**, *47*, 2029.
(54) Dittrich, B.; Harrowfield, J. M.; Koutsantonis, G. A.; Nealon, G. L.; Skelton, B. W. *Dalton Trans.* **2010**, *39*, 3433.
(55) Berven, B. M.; Koutsantonis, G. A.; Skelton, B. W.; Trengove, R. D.; White, A. H. *Inorg. Chem.* **2009**, *48*, 11832.
(56) Bruce, M. I.; Wong, F. S.; Skelton, B. W.; White, A. H. *J. Chem. Soc., Dalton Trans.* **1981**, 1398.
(57) Rillema, D. P.; Jones, D. S.; Levy, H. A. *J. Chem. Soc., Chem. Commun.* **1979**, 849.
(58) Noviandri, I.; Brown, K. N.; Fleming, D. S.; Gulyas, P. T.; Lay, P. A.; Masters, A. F.; Phillips, L. *J. Phys. Chem. B* **1999**, *103*, 6713.
(59) Fox, M. A.; Roberts, R. L.; Khairul, W. M.; Hartl, F.; Low, P. J. *J. Organomet. Chem.* **2007**, *692*, 3277.
(60) Schauer, P. A.; Low, P. J. *Eur. J. Inorg. Chem.* **2012**, *2012*, 390.
(61) Gendron, F.; Burgun, A.; Skelton, B. W.; White, A. H.; Roisnel, T.; Bruce, M. I.; Halet, J.-F.; Lapinte, C.; Costuas, K. *Organometallics* **2012**, *31*, 6796.
(62) Paul, F.; Ellis, B. G.; Bruce, M. I.; Toupet, L.; Roisnel, T.; Costuas, K.; Halet, J.-F.; Lapinte, C. *Organometallics* **2006**, *25*, 649.
(63) Gauthier, N.; Tchouar, N.; Justaud, F.; Argouarch, G.; Cifuentes, M. P.; Toupet, L.; Touchard, D.; Halet, J.-F.; Rigaut, S.; Humphrey, M. G. *Organometallics* **2009**, *28*, 2253.
(64) Smith, G.; Cole-Hamilton, D. J. *J. Chem. Soc., Dalton Trans.* **1984**, 1203.
(65) Smith, G.; Cole-Hamilton, D. J.; Thornton-Pett, M.; Hursthouse, M. B. *J. Chem. Soc., Dalton Trans.* **1985**, 387.
(66) Bruce, M. I.; Koutsantonis, G. A.; Liddell, M. J.; Tiekink, E. R. T. *J. Organomet. Chem.* **1991**, *420*, 253.
(67) Selegue, J. P. *J. Am. Chem. Soc.* **1983**, *105*, 5921.
(68) Iyer, R. S.; Selegue, J. P. *J. Am. Chem. Soc.* **1987**, *109*, 910.
(69) Johno, K.; Tanaka, Y.; Koike, T.; Akita, M. *Dalton Trans.* **2011**, *40*, 8089.
(70) Smith, M. E.; Flynn, E. L.; Fox, M. A.; Trottier, A.; Wrede, E.; Yufit, D. S.; Howard, J. A. K.; Ronayne, K. L.; Towrie, M.; Parker, A. W.; Hartl, F.; Low, P. J. *Chem. Commun.* **2008**, 5845.
(71) Wong, K. M.-C.; Lam, S. C.-F.; Ko, C.-C.; Zhu, N.; Yam, V. W.-W.; Roue, S.; Lapinte, C.; Fathallah, S.; Costuas, K.; Kahlal, S.; Halet, J.-F. *Inorg. Chem.* **2003**, *42*, 7086.
(72) Scott, A. P.; Radom, L. *J. Phys. Chem.* **1996**, *100*, 16502.
(73) McGrady, J.; Lovell, T.; Stranger, R.; Humphrey, M. *Organometallics* **1997**, *16*, 4004.
(74) Koentjoro, O.; Rousseau, R.; Low, P. *Organometallics* **2001**, *20*, 4502.
(75) Bruce, M. I.; Burgun, A.; Gendron, F.; Grelaud, G.; Halet, J.-F.; Skelton, B. W. *Organometallics* **2011**, *30*, 2861.
(76) Albers, M. O.; Liles, D. C.; Robinson, D. J.; Singleton, E. *Organometallics* **1987**, *6*, 2179.
(77) Balavoine, G. G. A.; Boyer, T.; Livage, C. *Organometallics* **1992**, *11*, 456.
(78) Valles-Pardo, J. L.; Guijt, M. C.; Iannuzzi, M.; Joya, K. S.; de Groot, H. J. M.; Buda, F. *ChemPhysChem* **2012**, *13*, 140.